Relationship of wheat yield with temperature in large irrigation areas of Sudan

スーダンの大規模灌漑地におけるコムギ収量と気温の関係

Abuelgasim Ibrahim Idriss Musa

2022

Relationship of wheat yield with temperature in large irrigation areas of Sudan

スーダンの大規模灌漑地におけるコムギ収量と気温の関係

Abuelgasim Ibrahim Idriss Musa

A thesis

submitted to the United Graduate School of Agricultural Sciences, Tottori University, in the partial fulfillment of the requirements for the degree of Doctor of Philosophy in Global Dryland Science

The United Graduate School of Agricultural Sciences

Tottori University, Japan

2022

Relationship of wheat yield with temperature in large irrigation areas of Sudan

スーダンの大規模灌漑地におけるコムギ収量と気温の関係

A Post Graduate Thesis submitted to The United Graduate School of Agricultural Sciences, Tottori University as partial fulfillment of the requirement for the award of Doctor of Philosophy in Global Dryland Science.

Abuelgasim Ibrahim Idriss Musa

Major Supervisor:

Prof. Mitsuru Tsubo

Professor, Arid Land Research Center,

Tottori University, Tottori, Japan

Co-Supervisors:

Prof. Yasunori Kurosaki

Professor, Arid Land Research Center,

Tottori University, Tottori, Japan

Prof. Yasuomi Ibaraki

Professor, Faculty of Agriculture, Yamaguchi University,

Yamaguchi, Japan

DEDICATION

This thesis work is dedicated to my wife, Marwa, who has been a constant source of support and encouragement during graduate school and life challenges. I am genuinely thankful for having you in my life. This work is also dedicated to my mother's soul and my father, who has always loved me unconditionally and whose good examples have taught me to work hard for what I aspire to achieve.

Acknowledgments

First and foremost, I am incredibly grateful to my supervisors, Prof. Mitsuru Tsubo, Prof. Yasunori Kurosaki, and Prof. Yasuomi Ibaraki, for their invaluable advice, continuous support, and patience during my Ph.D. study. Their immense knowledge and great experience have encouraged me in my academic research and daily life.

My thanks go to the management and Staff of JICA for funding my study and Sudan Meteorological Authority for nominating me for the Ph.D. program and providing the necessary support.

I am sincere to Dr. Izzat Sidahmed and the Agriculture Research Corporation for providing datasets and support during the research. The thanks also go to Professors Faisal El-Hag and Imad-Eldin Ali-Babiker for their continuous support.

I would like to sincerely thank Dr. Shaoxiu Ma, Prof. Nigussie Haregeweyn, and all professors and staff members in the Arid Land Research Center. Their kind help and support have made my study and life in Japan a wonderful time. I would also like to thank Dr. Yasir Gorafi and Dr. Nasreen Kamal for their various types of support during my study. I want to thank my friends and lab mates for a cherished time spent together in the lab and social settings. Finally, I would like to express my gratitude to my parents, wife, and children. Without their tremendous understanding and encouragement over the past three years, it would be impossible for me to complete my study.

Table of Contents

List of Tables

List of Figures

List of Abbreviations

Chapter 1
General Introduction

1.1. Background

Drylands are most sensitive to climate change; global warming over the past century is higher in drylands than in wetlands (Huang et al. 2016). Further, temperatures in drylands would increase by 3°C under the 1.5 °C mean global warming scenario, and their areas would tend to increase in the future (Huang et al. 2017). In dryland agro-ecosystems, the effect of climate variability on crop production under changing climate needs to be understood.

Recent climate change has been reducing crop production in many parts of the world including Africa (IPCC 2014, 2019). Temperature tends to increase over Sub-Saharan Africa (Gil-Alana et al. 2019), and increasing trends in maximum and minimum temperatures are most likely associated with increasing trends in warm days and nights (Omondi et al. 2014; Ongoma and Chen 2017; Gebrechorkos et al. 2019) in both arid and tropical regions (Elagib 2010; Mengistu et al. 2014; Nsubuga et al. 2014). In countries vulnerable to climate change, temperature increases would impact field crop production (Hatfield et al. 2011; Hatfield and Prueger 2015), particularly that of wheat (*Triticum aestivum*), a major cereal that is normally grown under cool climate. The first step toward wheat adaptation is to understand the historic relationship between crop productivity and temperature variability (Iizumi et al. 2018; Ray et al. 2019).

Crop yield estimation is required for the process of decision-making in food policy on a regional scale. For example, the outlook for cereal production prior to harvest is crucial for the government decision-makers to plan grain imports beforehand in case of shortages. Further, crop yield prediction using seasonal weather forecasts can help in coping with climate-related risks by taking mitigation measures. Thus, early warning systems for climate risk management in crop production have gained worldwide attention, as they can provide useful crop yield information based on seasonal weather forecasts (Asfaw et al. 2018). However, the current spatial resolution of the forecast data is not high enough for operational use in estimating crop yield.

High spatial resolution climate data are required for local-scale impact assessments of climate variability and changes of ecosystem services. The outputs of general circulation models (GCMs)

are not sufficient for such local-scale studies, and therefore regional climate models (RCMs), which incorporate detailed specifications of the earth's surface such as land use and water bodies, have been broadly applied to satisfy this requirement. RCMs outperform GCMs in detailed simulation of mesoscale processes, e.g., convective rainfall processes (Wilby and Wigley 1997; Soares et al. 2012; Garcia-Carreras et al. 2015). Weather Research and Forecasting (WRF) is a well-known RCM used for many purposes such as operational forecasting and dynamical downscaling. As local climates are regulated by global circulations and further constrained by land surface conditions, the WRF model provides multiple physics options to satisfy region-dependent climate conditions (Figure 1.1). Numerous studies have been conducted with the aim of identifying robust configurations of physical processes for specific scales and geographical locations and their applications (Fu et al. 2005; Christensen et al. 2007; Giorgi et al. 2009; van der Linden and Mitchell JFB 2009; Mearns et al. 2012; Solman et al. 2013). The WRF model has been worldwide adapted to generate high spatial climate information for various studies of climate impacts in different regions.

Wheat is one of the most important grains in the world and contributes significantly to food security in many countries. The demand for wheat production is increasing due to the increase of the world's population, and so does Sudan. Crop growing seasons in Sudan depend on temperature and rainfall. While the lack of rainfall has a negative impact on summer crops, high temperature has a negative impact on wheat during the dry season. Iizumi et al. (2021) have reported that crop yield projections for the future global average temperature warming of 1.5 to 4.2 °C indicate that the domestic production share of wheat in Sudan could decrease from the current 16% to 4.5–12.2% by 2050, and hence it is essential to increase the yields by up to 4.7% per year in order to maintain the current domestic production share through different adaptation measures to global warming. While improving the heat tolerance of wheat varieties is one of the reliable measures to adapt to climate change and increasing climate variability, a wheat yield outlook system with high spatial resolution data of seasonal forecasts is also a valuable tool to cope with climate variability under changing climate.

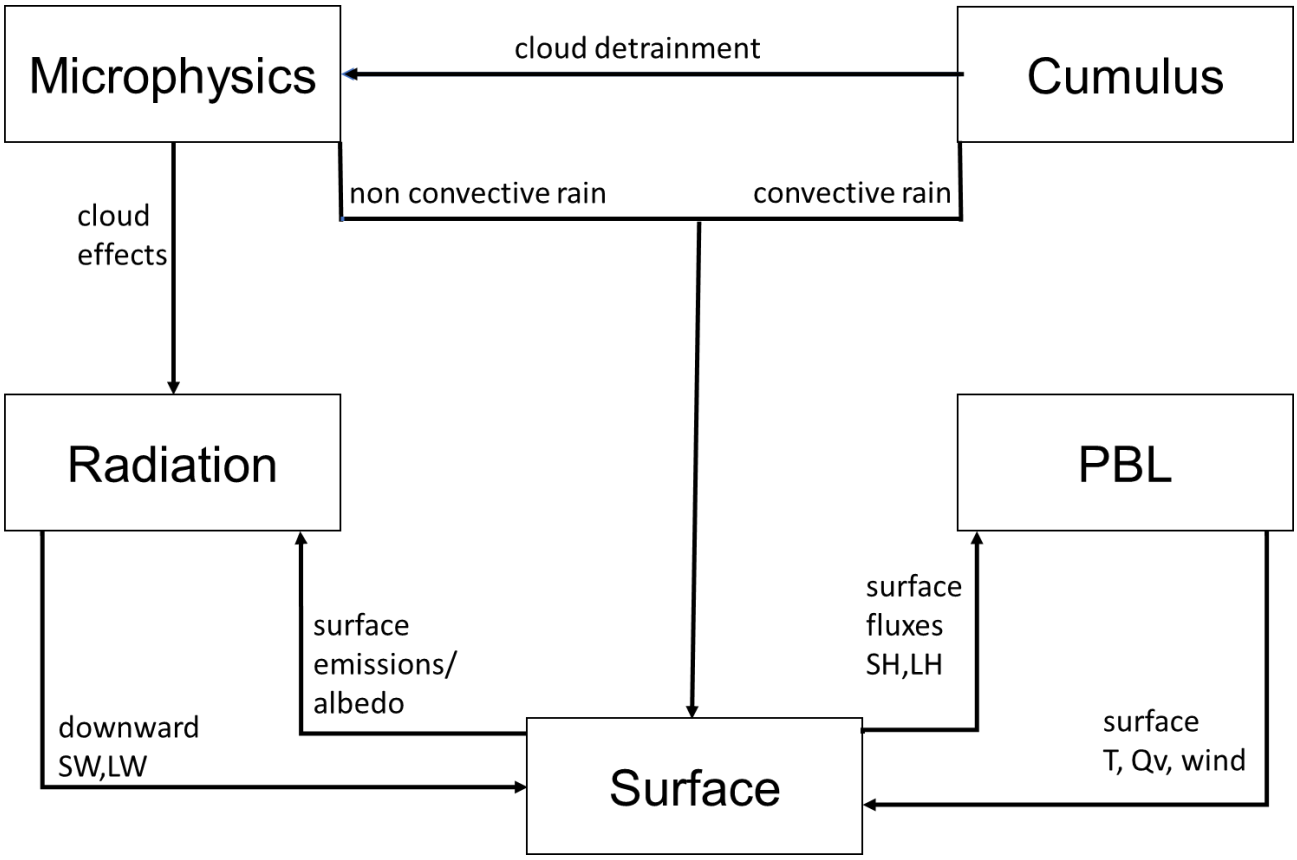

Figure 1.1 A schematic diagram of physics options and their interactions within a typical numerical weather prediction model [redrawn Fig. 2 of Dudhia (2014)]. (PBL indicate Planetary Boundary Layer, SW and LW indicate shortwave and longwave radiation, respectively, LH and SH and are the latent heat and sensible heat fluxes, respectively, and T and Qv are the mean temperatures and water vapor mixing ratios)

1.2. Study aim

Sudan is one of the most vulnerable countries to climate variability and change. In particular, agriculture is affected by climate hazards such as drought in summer and extremely high temperatures in winter. To cope with such hazards, farmers need timely and reliable climate information for agronomic management, including seed planting, fertilizer application, and irrigation scheduling. The interpretation of seasonal climate forecasts is important as a way to

project crop yield before the growing season. In Sudan, wheat is one of the most important grains, and its cultivation is carried out under irrigation during the hot and dry season. The aim of this thesis is therefore to develop an approach for crop yield prediction with regard to the impact of high temperature on wheat production. The main objectives are (1) to investigate the regional-scale relationship of wheat yields with temperature for the last five decades, (2) to identify a robust configuration of the WRF model for generating high-spatial-resolution climate data for crop growing seasons, and (3) to study the feasibility of wheat yield forecasting. Thus, the thesis is structured as the following main chapters: statistical analysis of yield and temperature relationship (Chapter 2), dynamical downscaling of climate variables (Chapter 3), and forecasting the yield production anomaly with statistical model (Chapter 4).

Chapter 2

Statistical Analysis of Yield and Temperature Relationship

2.1. Introduction

Case studies on wheat yield trends and temperature variations have been reported from various countries (You et al. 2009; Brisson et al. 2010; Licker et al. 2013; Tack et al. 2015; Asseng et al. 2017; Morgounov et al. 2018). Yield loss of winter wheat in Kansas (USA) in 1985–2013 largely resulted from freezing temperatures in fall and extreme heat in spring during the growing season from September to May (Tack et al. 2015). In China, wheat yield decreased by 4.5% in 1979–2000 (You et al. 2009). Under rainfed conditions, an 11% yield decline in 1973–2010 was reported in Picardy (France), a vital winter wheat-producing region in Europe, where maximum spring temperatures increased by 2.4 °C and total fall precipitation decreased by 9% over the study period (Licker et al. 2013). Rainfed spring wheat in Eurasia and North America is harmed by high temperature in June and July, when heading, flowering, and ripening occur (Morgounov et al. 2018). In regions where spring wheat is grown under irrigation, such as India, higher mean growing-season temperature is associated with lower yield (Asseng et al. 2017). According to model simulation at a global scale (Asseng et al. 2015), wheat production would fall by 6% for each degree of temperature increase.

Wheat production is considerably reduced by temperatures above the optimum. According to Porter and Gawith (1999), the optimum temperature for wheat is around 20 °C, ranging between 17 °C and 23 °C; plants stop to grow below 0 °C or above 37 °C, and die at around − 17 °C or 47.5 °C. Increased daytime and nighttime temperatures decrease wheat yields in controlled environments (Prasad et al. 2008; Garcia et al. 2015; Garcia et al. 2016; Narayanan et al. 2015; Nuttall et al. 2018). The exposure of wheat plants to daytime temperatures ≥ 35 °C during anthesis decreases grain yield (Nuttall et al. 2018), and additional exposure to high nighttime temperature further decreases it (Narayanan et al. 2015). Nighttime temperature ≥ 20 °C from booting to maturity shortens grain filling duration, hence reducing yield (Prasad et al. 2008). Similar responses to high night temperature have been found under field conditions from stem elongation to anthesis (Garcia et al. 2015) and from post-anthesis to maturity (Garcia et al. 2016). High temperature during grain-filling decreases yield in wheat-producing regions with a hot climate, such as Sudan (Ishag and Mohamed 1996).

The effect of climate change is particularly severe in Sub- Saharan Africa, and the Sudano-Sahelian countries could experience a considerable loss of agricultural production (Calzadilla et al. 2013). Sudan is one of the most important irrigated wheat producers in the region; its climate is characterized by high temperature and low humidity (Negassa et al. 2013). Wheat production in this hot region will deteriorate in the future (Asseng et al. 2017), and heat-resistant cultivars need to be improved to meet the future demand in the country. The only study (Adam and Ageeb 1994) that reported on the relationship between wheat yields and temperature in Sudan analyzed a single area, the Gezira Scheme, during a short period (10 crop seasons from 1981/82 to 1991/92).

Although wheat yields in Sudan are low due to a combination of constraints such as high temperature, short growing season, low fertilizer input, and low soil carbon content, we focus on temperature in this study. The main objective of this study was to investigate the regional-scale relationship of wheat yields with temperature in Sudan for the last five decades. The specific objectives were to (1) evaluate recent trends in annual temperature, (2) analyze time series trends in temperature during the wheat growing season, and (3) determine how yield is associated with growing-season temperature. We also discussed the future trends in the effect of climate change on yields. To the best of our knowledge, this is the first study to investigate the yield–temperature relationship in Sudan using long-term observed data.

2.2. Methods

2.2.1. Study area

Three major wheat-producing areas in Sudan were selected: Northern State (northern region), Gezira State (central region), and Kassala State (eastern region) (Figure 2.1). They cover about 80% of the wheat cultivation area and account for about 85% of domestic production (FAO 2019). Spring-type wheat is cultivated under irrigated conditions in the relatively cold, dry season. Irrigated fields are located along the Nile River in Northern State, the Blue Nile River in Gezira State on the central clay plain, and the Atbara River in Kassala State.

Data from three meteorological stations were used: Dongola (19.17°N, 30.48°E) in Northern State, Wad Medani (14.40°N, 33.48°E) in Gezira State, and New Halfa (15.32°N, 35.60°E) in Kassala State (Figure 2.1). They lie on flat land (elevations a.s.l.: Dongola, 226 m; Wad Medani, 408 m;

and New Halfa, 462 m) and are representative of the study areas. Dongola is located in a hyper-arid region with an annual rainfall of < 15 mm and an annual potential evapotranspiration (PET) of about 2300 mm. Wad Medani and New Halfa are located in arid regions with an annual rainfall of 250–300 mm and an annual PET of 1950–2250 mm (Elagib and Mansell 2000). According to the FAO (2012) soil classification, Arenosols, Fluvisols, Leptosols, and Vertisols are found in Northern State; mainly Vertisols and, in small areas, Luvisols in Gezira State; and Luvisols, Cambisols, and Vertisols in Kassala State.

2.2.2. Data collection and processing

Wheat crop data of the study areas were obtained from the Ministry of Agriculture and Natural Resources of Sudan. The time series data of wheat production (kg) and harvested area (ha) for 48 years (1970/71–2017/18 crop seasons) were used. The year-by-year grain yields (kg/ha) were calculated as the production divided by the harvested area. No data were available for Gezira and Kassala states in 1984/85 and for Kassala State in 2006/07, 2008/09, and 2009/10.

The regional-scale yield shows a reasonable agreement with the plot-scale yield at research stations and if the two types of yield are compared for the overlapped period (2015/16 and 2016/17); the yields of the major varieties, i.e., Imam, Debeira, Wad Elneel, and Zakia, in 2015/16 and 2016/17 range between 1800 and 6100 kg/ha at Gezira Research Station and between 1300 and 4500 kg/ha at New Halfa Research Station (Tahir et al. 2018).

Daily maximum and minimum temperature data at the three meteorological stations for 1970–2018 were obtained from the Sudan Meteorological Authority. Prior to the data processing, the homogeneity test of the temperature time series data was conducted to detect the changepoints using RHtestsV4, software developed by the Joint CCl/Clivar/ JCOMM Expert Team on Climate Change Detection and Indices (Wang and Feng 2013); detected changepoints of the minimum temperature time series data at Wad Medani and New Halfa were adjusted using a provision of Quantile- Matching (QM) included in the software.

Annual and monthly averages of daily maximum temperature (annual and monthly TMAX, respectively) and daily minimum temperature (annual and monthly TMIN, respectively) were calculated. Also, extreme temperature indicators of hot days (maximum temperature > 35 °C) and

hot nights (minimum temperature > 20 °C) (Collins et al. 2000) were used. The ratio of hot days to the number of days in a month (monthly THD) and the ratio of hot nights to the number of days in a month (monthly THN) were calculated using ClimPACT2, software introduced by the Commission for Climatology Expert Team on Sector-specific Climate Indices of the World Meteorological Organization. In Sudan, wheat is typically planted in November, heading and flowering occur in January, and the ripening period is mainly February; November–February was defined as the growing season in this study. Means of daily maximum and minimum temperatures for the 4 months (growing-season TMAX and TMIN, respectively) and the ratios of hot days and hot nights to the number of days in the 4 months (growing-season THD and THN, respectively) were calculated.

2.2.3. Data analysis

To determine the trends of the temperature indicators (TMAX, TMIN, THD, and THN), linear regression analysis over time was carried out. To determine whether a time series had a monotonic upward or downward direction, the temperature indicators were further tested using the nonparametric Mann–Kendall and Sen's slope estimator tests. The trend lines from regression analysis were used to analyze the yield–temperature relationship. Increasing yield trends could be expected owing to newly released cultivars, increased use of quality seeds, increased inorganic fertilizer application, and better irrigation and technology dissemination (Faki et al. 1994; Tahir et al. 2000; Tahir et al. 2020a). A detrending approach (Nicholls 1997) was used to remove the effect of agricultural development: time series data of the yields were detrended as deviations (anomalies) from regression lines detected at a significance level of 5%. All the temperature indicators with significant trends were detrended using the regression lines; in the absence of a trend, anomalies from the means over the period were used. The relationships between the detrended yields and temperature indicators were analyzed by correlating the anomalies using Pearson's correlation and nonparametric Spearman's rank correlation. Prior to the correlation analyses, the Shapiro–Wilk normality test was conducted to detect whether the yield anomalies were normally distributed and therefore the detrended procedure functioned validly; all the datasets met the assumption of normality at $p \leq 0.05$.

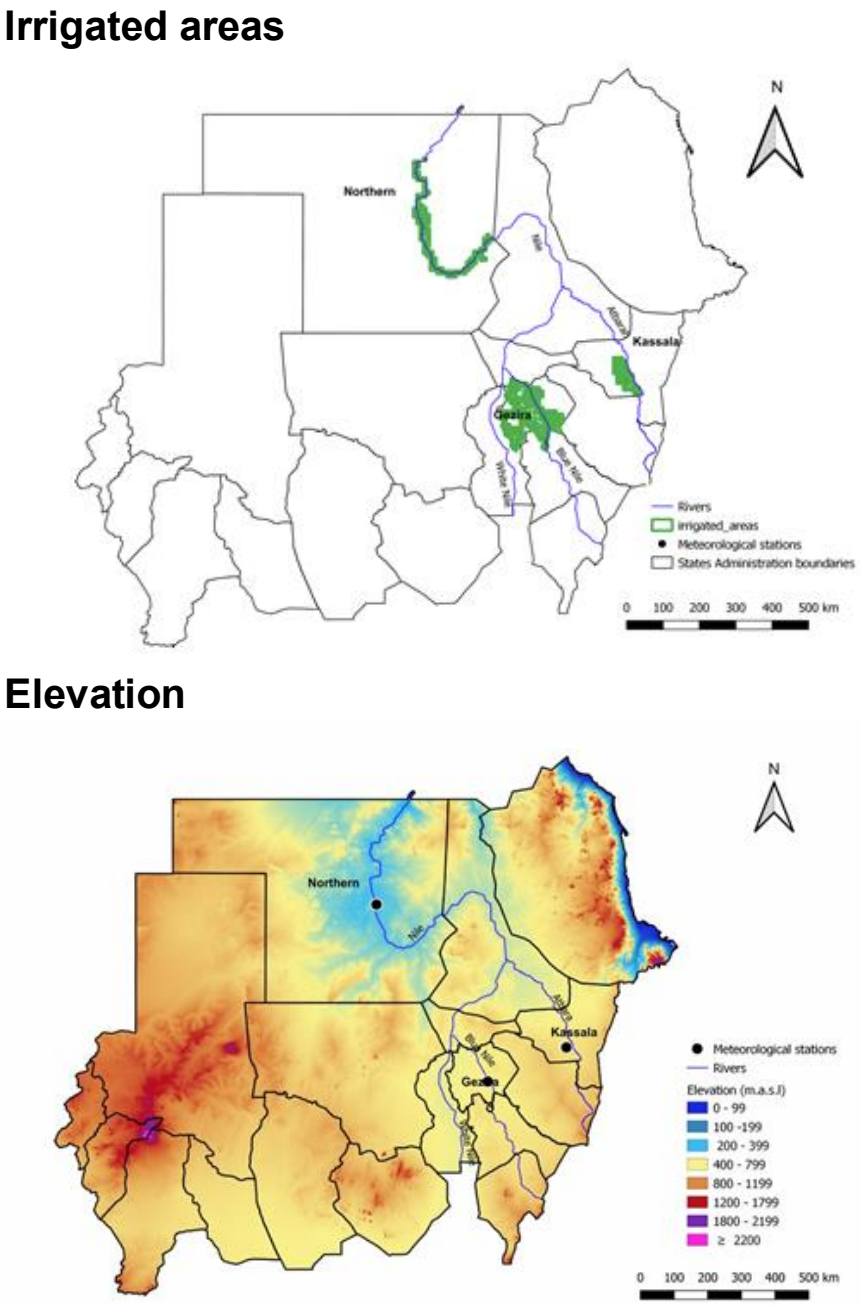

Figure 2.1 Three major wheat-producing (irrigated) areas of Sudan (Northern State, Gezira State, and Kassala State) and their representative meteorological stations (Dongola, Wad Medani, and New Halfa, respectively)

Counterfactual yield is the estimated yield what would occur without warning and derived by inputting detrended temperature data to the established yield–temperature relationships. To calculate the counterfactual yields, (i) 5-year moving averages of the original yields and growing-season mean temperatures (growing-season averages of daily mean temperature = average of daily TMAX and TMIN) were calculated; (ii) temperature increments relative to 1970/71 over the period were calculated using linear equations, with which the 5-year moving averages were fitted; (iii) yield changes relative to 1970/71 were calculated by substituting the temperature increments into equations of linear regression between the anomalies of growing-season mean temperatures and the original yields from the 5-year moving averages; and (iv) yield changes were subtracted from the original yield. This approach is essentially similar to the methods used in the previous studies (Lobell and Field 2007; Lobell et al. 2011; Moore and Lobell 2015). All data analyses were conducted in MS Excel, SPSS v. 25, and R v. 3.6.1 software.

2.3. Results

2.3.1 Maximum and minimum temperatures

Annual TMIN and TMAX trends for 1970–2018 at the three meteorological stations are shown in Figure 2.2. Annual TMIN had increasing trends ($p \leq 0.05$); slopes of the regression lines indicated a higher increase per decade at Dongola (0.83 °C) than at Wad Medani (0.50 °C) and New Halfa (0.31 °C). Annual TMAX had increasing trends at Dongola (0.23 °C) and Wad Medani (0.25 °C) ($p \leq 0.05$), but not at New Halfa. The Mann–Kendall and Sen's slope estimator tests also detected monotonic upward trends in both TMAX and TMIN at all locations ($p \leq 0.05$), except for TMAX at New Halfa. The highest daily TMAX during the study period was 49.8 °C at Dongola on 24 June 2010, 47.4 °C at Wad Medani on 27 May 1991, and 47.5 °C at New Halfa on 25 May 1998. The lowest daily TMAX was 16.2 °C at Dongola on 29 January 1983, 20.3 °C at Wad Medani on 26 December 1992, and 20.5 °C at New Halfa on 10 January 1990. The highest daily TMIN was 35.0 °C at Dongola on 18 May 2016, 32.6 °C at Wad Medani on 7 May 2009, and 34.7 °C at New Halfa on 30 April 2011. The lowest daily TMIN was 1.0 °C at Dongola on 9 February 1982, 4.1 °C at Wad Medani on 25 December 1971, and 4.8 °C at New Halfa on 6 February 1983.

2.3.2 Growing-season temperature indicators

The distribution of monthly TMAX and TMIN is shown in Figure 2.3. Among the median values

at Dongola, the highest TMAX was in June and the highest TMIN was in August. At Wad Medani and New Halfa, the highest TMAX was in May and the highest TMIN in June. All locations had the lowest monthly TMAX and TMIN (medians) in January, followed by December and February. Linear regression analysis (data not shown) revealed monthly TMAX and TMIN trends for the growing season. Dongola had increasing trends in TMIN in all months ($p \leq 0.05$) and in TMAX in November only ($p \leq 0.05$). Wad Medani had a monthly TMAX increase over the entire period ($p \leq 0.05$) except January, and increasing trends in TMIN in December, January, and February. New Halfa had increasing trends in TMIN over the entire period ($p \leq 0.05$) except January and no trends in TMAX. In the Mann–Kendall and Sen's slope estimator tests (Table 2.1), Dongola had the same results for TMIN, but a monotonic upward trend in TMAX in December instead of November. Wad Medani had monotonic upward trends in TMAX in November and December but not in January or February, and increasing trends in TMIN in all months except January. New Halfa had the same results (no trends) for TMAX, but monotonic upward trends for TMIN over the entire period ($p \leq 0.05$).

Linear trends in the growing-season TMAX and TMIN are shown in Figure 2.4. All three locations had increasing trends in both TMAX (decadal increase of 0.26 °C, 0.37 °C, and 0.20 °C for Dongola, Wad Medani, and New Halfa, respectively) and TMIN (0.71 °C, 0.40 °C, and 0.40 °C) (all $p \leq 0.05$). In the nonparametric tests, both TMAX and TMIN had monotonic upward trends at all three locations, except for TMAX at Dongola (Table 2.1).

During the growing season, the highest daily TMAX recorded at Dongola was higher in November (41.5 °C) and February (42.4 °C) than in December (37.6 °C) and January (39.0 °C). In contrast, the highest daily TMIN was higher in December (34.0 °C) and January (33.5 °C) than in November (26.0 °C) and February (24.0 °C). At both Wad Medani and New Halfa, the highest daily TMAX was above 40 °C and TMIN was above 26 °C in November–February. All records were higher than the thresholds (35 °C for hot days and 20 °C for hot nights).

In Dongola, monthly THN had increasing trends in November and December ($p \leq 0.05$) in both ?the linear regression and nonparametric analyses and THD had a monotonic upward trend in November (Table 2.1). In Wad Medani, monthly THD had upward trends ($p \leq 0.05$) except in

November in both the linear regression and nonparametric analyses, and monthly THN had an increasing trend in February ($p \leq 0.05$) in linear regression analysis but no trend in nonparametric tests (Table 2.1).

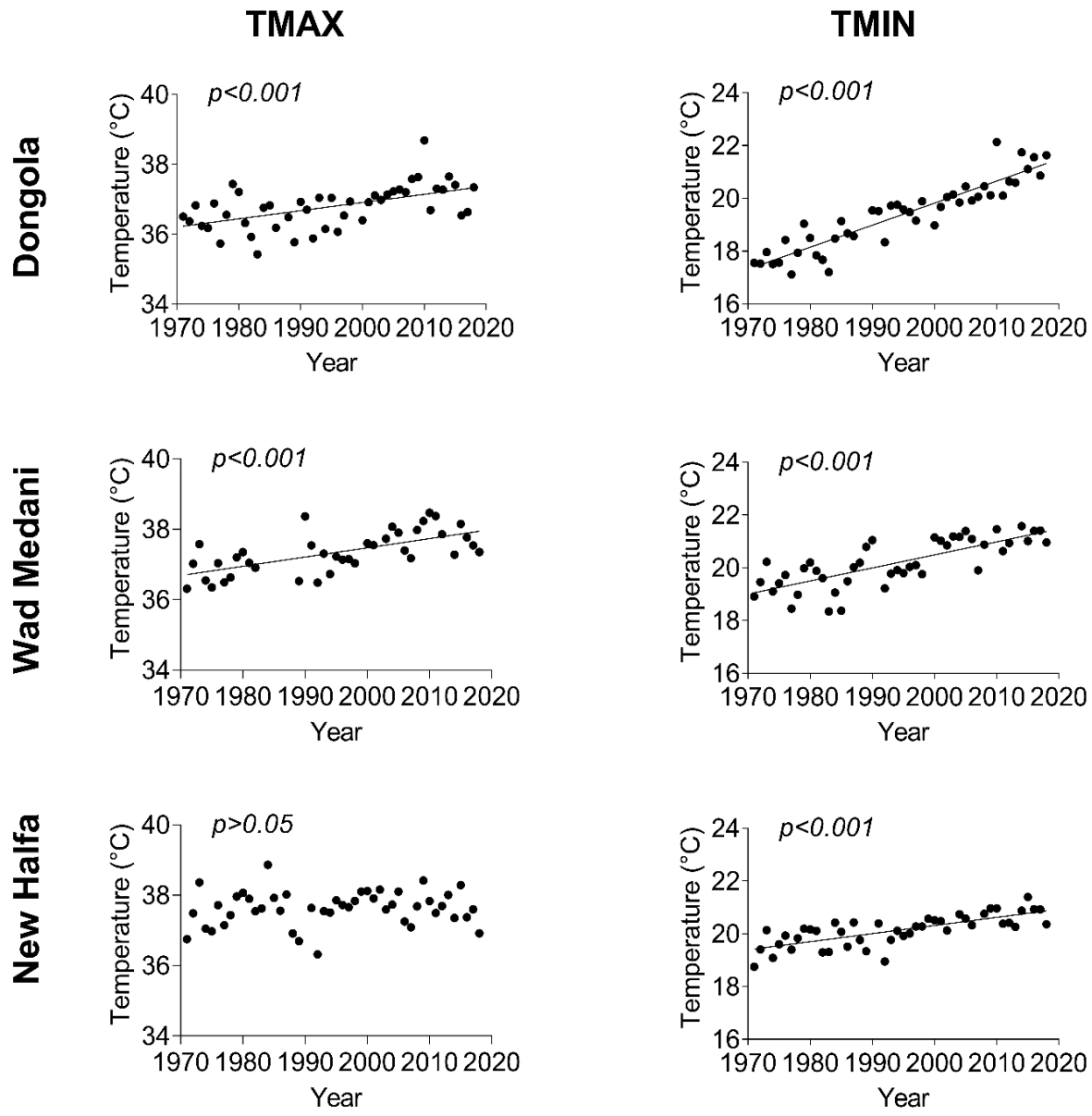

Figure 2.2 Linear trends in annual average daily maximum (TMAX) and minimum temperatures (TMIN) from 1970 to 2018 at the Dongola, Wad Medani, and New Halfa meteorological stations in Sudan. Linear lines (estimated by least squares regression) in the figures are significant increasing trends in TMAX and TMIN

In New Halfa, THN had an increasing trend in November in both the linear regression and nonparametric analyses (Table 2.1) ($p \leq 0.05$) and in February in linear regression analysis ($p \leq 0.05$). Growing-season THD and THN had increasing trends at all three locations ($p \leq 0.05$), except for THD at New Halfa, whereas nonparametric analysis detected monotonic upward trends in all cases (Table 2.1).

2.3.3. Relationships between yields and growing-season temperature indicators

The yield trends for the study period are shown in Figure 2.5. All study areas had increasing trends ($p \leq 0.05$). Kassala State had the highest increase rate (23 kg/ha per year), followed by Gezira State (21 kg/ha per year) and Northern State (18 kg/ha per year). In Northern State, the yield dropped sharply in the 2007/08 season and was consistently below the trend line until 2016/17 so that additional linear regression analysis for 1970/71 to 2006/07 revealed a remarkable increasing trend (45 kg/ha per year) before a decline started in 2007/08 (Figure 2.5). The original yields were lower than the counterfactual yields, and the differences increased from the 1970s to the 2010s in all study areas (Figure 2.6). In the 1970s, the original yields were lower than the counterfactual yields on average by 1% in Northern and Gezira states and by 2% in Kassala State, and the differences increased in the 2010s (7%, 12%, and 9%, respectively).

Pearson's correlation and Spearman's rank correlation between detrended yields (anomalies in Figure 2.5) and the temperature indicators (detrended) are shown in Table 2.2. In Northern State/Dongola, yield was negatively correlated with November THN and February TMAX (Pearson's correlation) and November THN (Spearman's rank correlation). Additional analysis for the period prior to 2007/08 showed negative correlation of yield with February TMIN ($r = -0.43$, $\rho = -0.33$) and THN ($r = -0.43$, $\rho = -0.61$), and with November THN ($\rho = -0.41$), December THN ($\rho = -0.53$), and January THN ($\rho = -0.63$) ($p \leq 0.05$). In Gezira State/Wad Medani, yield was negatively correlated with January TMAX. In Kassala State/New Halfa, yield was negatively correlated with several temperature indicators, particularly with November TMIN and February THN. Better yield–temperature relationships were found with the growing-season temperature indicators (Table 2.2). In Northern State/Dongola, yield was negatively correlated with the growing-season THN ($r = -0.41$, $\rho = -0.38$), and the same result was found for the period prior to 2007/08 ($r = -0.41$, $\rho = -0.52$). In Gezira State/Wad Medani, yield was negatively correlated

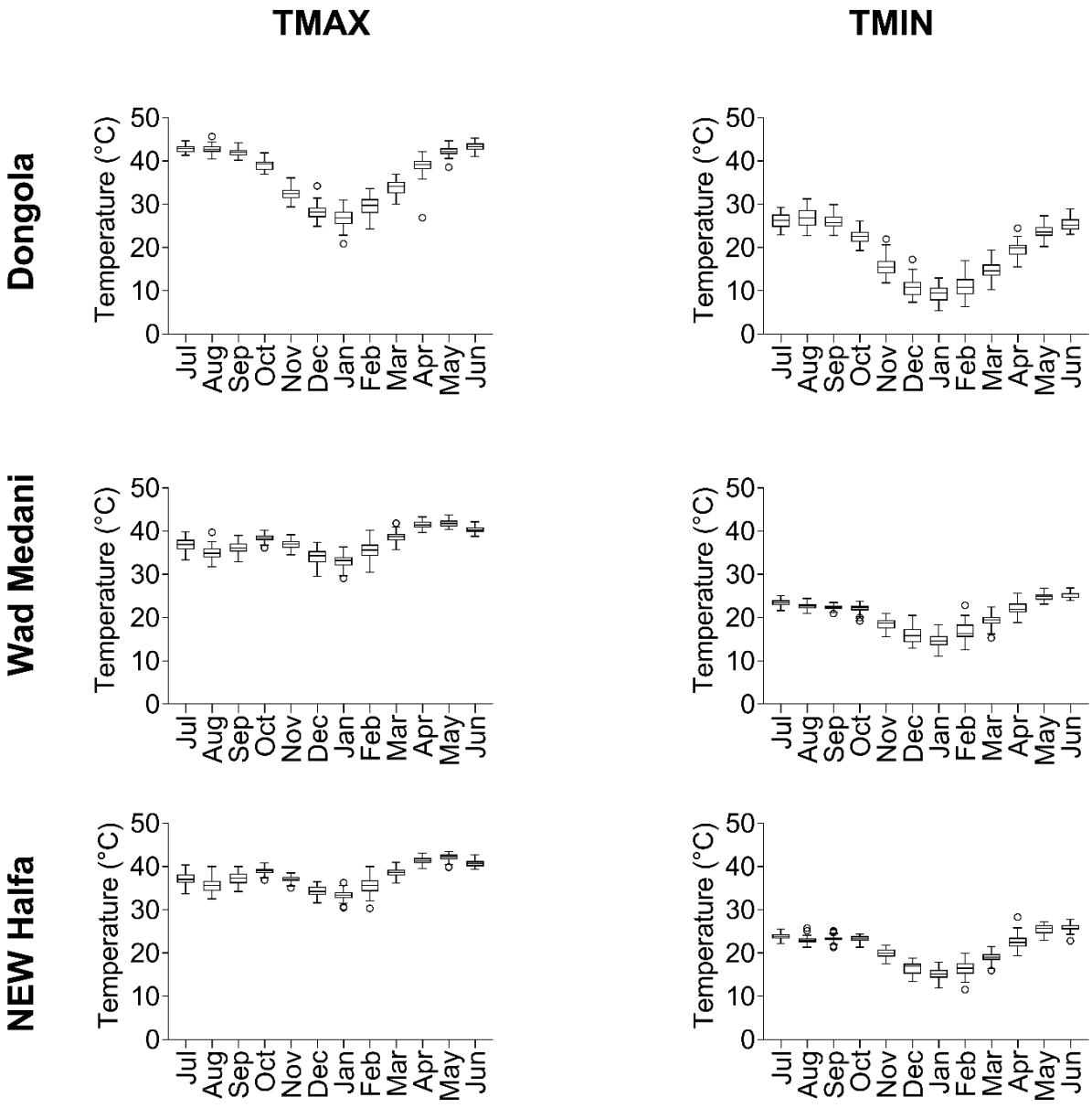

Figure 2.3 Box-and-whisker plots of monthly average daily maximum (TMAX) and minimum temperatures (TMIN) for from 1970 to 2018 at the Dongola, Wad Medani, and New Halfa meteorological stations in Sudan. Each box indicates the lower and upper quartiles, the horizontal line in the box represents the median, and the whiskers (vertical lines) denote the minimum and maximum values, excluding outliers (circles)

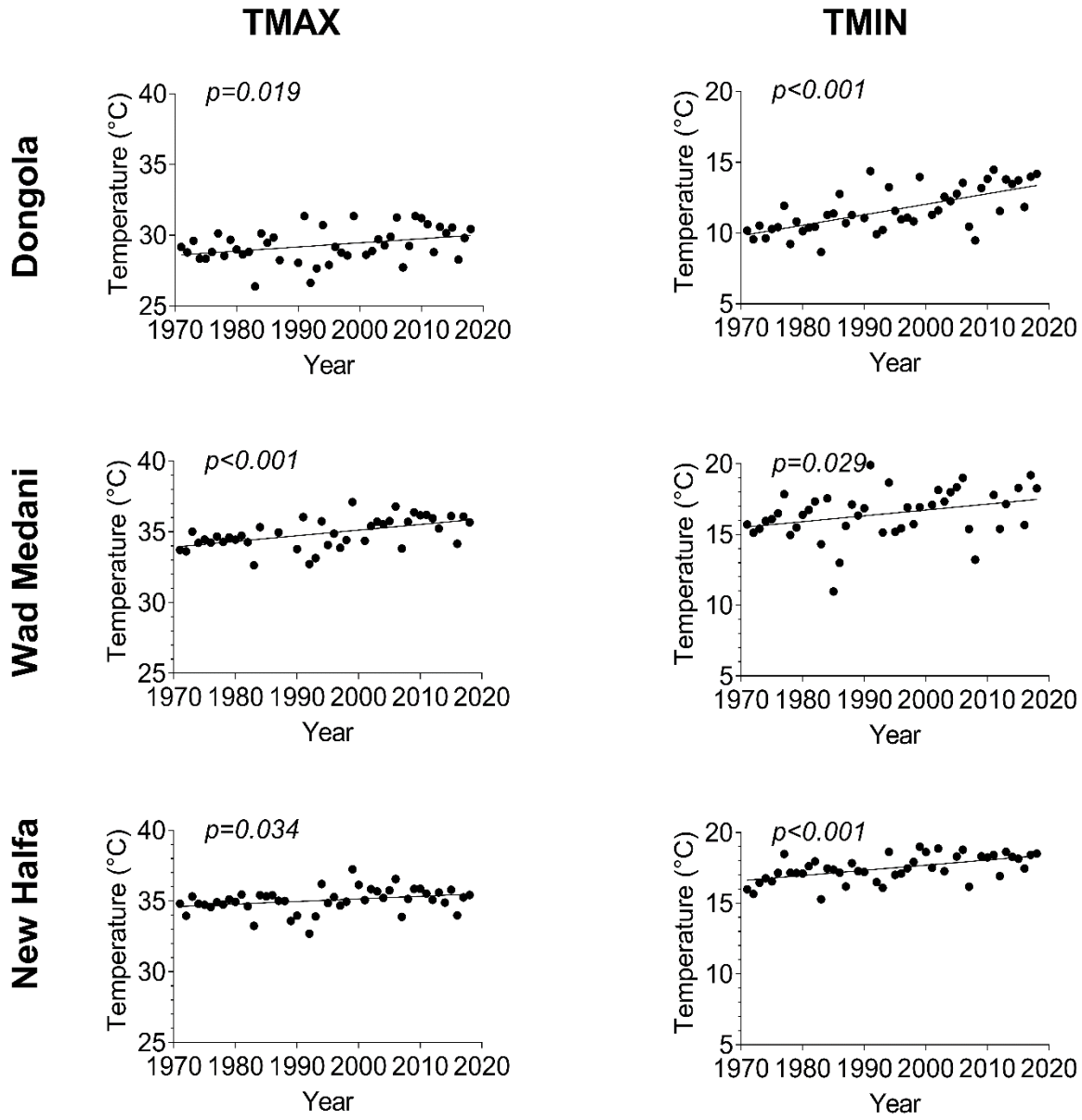

Figure 2.4 Wheat growing-season (November–February) average daily maximum (TMAX) and minimum temperatures (TMIN) from 1970 to 2018 at the Dongola, Wad Medani, and New Halfa meteorological stations in Sudan. Linear lines (estimated by least squares regression) in the figures are significant increasing trends in TMAX and TMIN

Table 2.1 Mann–Kendall (Z statistic) and Sen's estimator tests for monthly temperature indicators during wheat growing season in 1970–2018 at 3 meteorological stations in Sudan. TMAX, maximum temperature; TMIN, minimum temperature; THD, proportion of hot nights in a month

Station	Temperature indicator	November		December		January		February		Season	
		Z	*p*-value	*Z*	*p*-value	*Z*	*p*-value	*Z*	*p*-value	*Z*	*p*-value
Dongola	TMAX	1.82	0.07	2.47	0.01	0.86	0.39	1.25	0.20	1.87	0.06
	TMIN	4.78	< 0.01	4.50	< 0.01	3.39	< 0.01	3.75	< 0.01	5.15	< 0.01
	THD	2.02	0.04	1.23	0.21	0.67	0.50	1.06	0.28	2.21	0.02
	THN	2.29	0.02	1.96	0.04	0.46	0.60	1.51	0.12	2.52	0.01
Wad Medani	TMAX	2.57	0.01	2.89	< 0.01	1.56	0.11	1.84	0.06	3.43	< 0.01
	TMIN	2.97	0.02	4.44	<0.01	1.50	0.13	2.59	<0.01	3.43	<0.01
	THD	1.18	0.23	4.99	<0.01	2.11	0.03	2.08	0.03	3.17	< 0.01
	THN	1.46	0.14	1.54	0.12	0.83	0.40	1.58	0.11	2.38	0.01
New Halfa	TMAX	1.30	0.19	1.53	0.12	1.07	0.20	1.48	0.13	2.57	0.01
	TMIN	2.95	<0.01	2.52	0.01	2.22	0.02	3.11.	<0.01	3.41	< 0.01
	THD	-0.23	0.81	1.28	0.20	0.8	0.40	1.31	0.18	2.04	0.04
	THN	2.38	0.01	1.31	0.18	0.59	0.55	1.82	0.06	3.06	<0.01

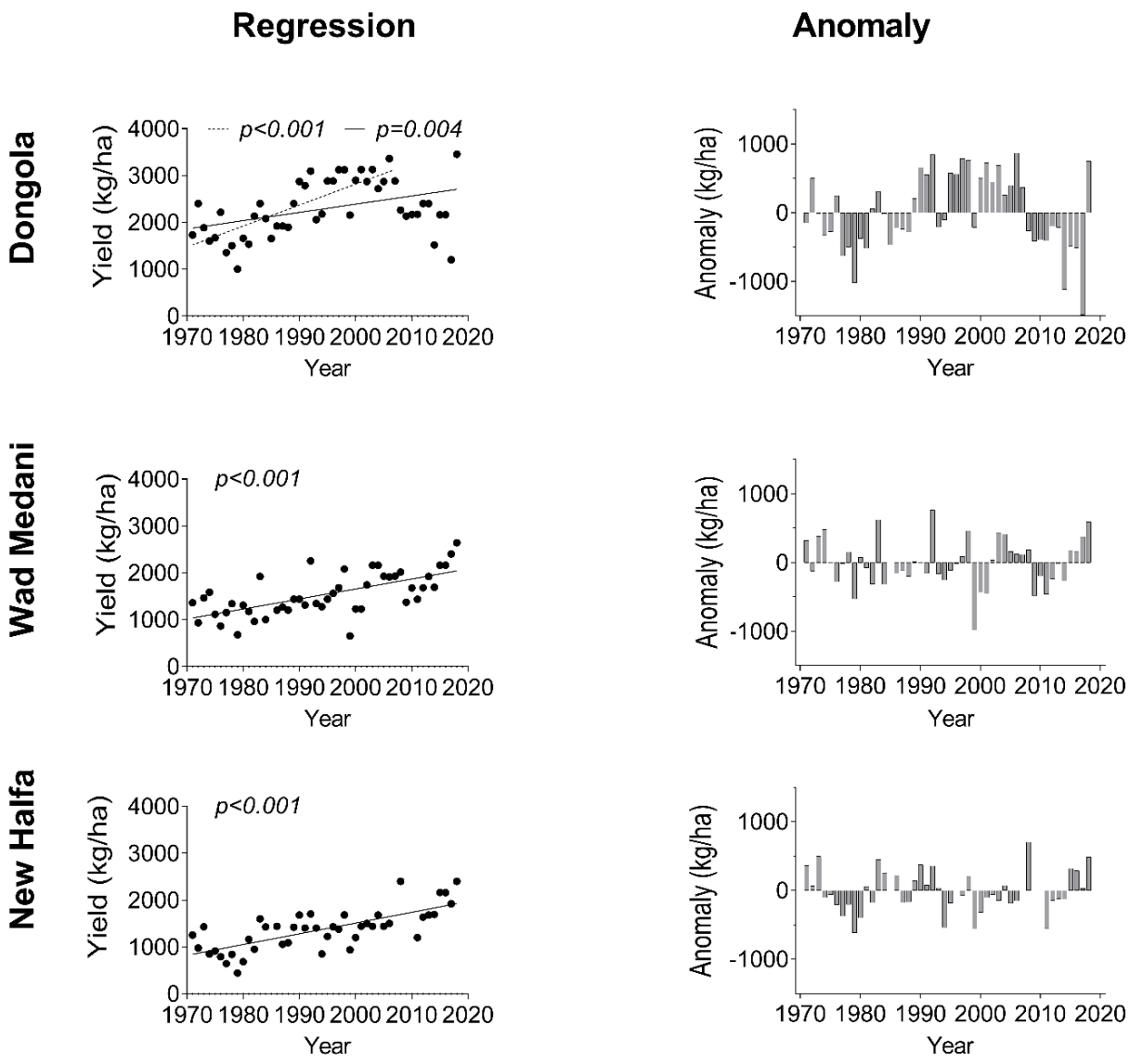

Figure 2.5 Irrigated wheat yield in the 1970/71 to 2017/18 seasons in Northern State, Gezira State, and Kassala State, Sudan and their anomalies from regression lines. Linear lines (estimated by least squares regression) in the figures are significant in Irrigated wheat yield in the 1970/71 to 2017/18 seasons in Northern State, Gezira State, and Kassala State, Sudan and their anomalies from regression lines. Linear lines (estimated by least squares regression) in the figures are significant increasing trends in the yield. For Northern State, the dashed regression line for 1970/71–2006/07 was used

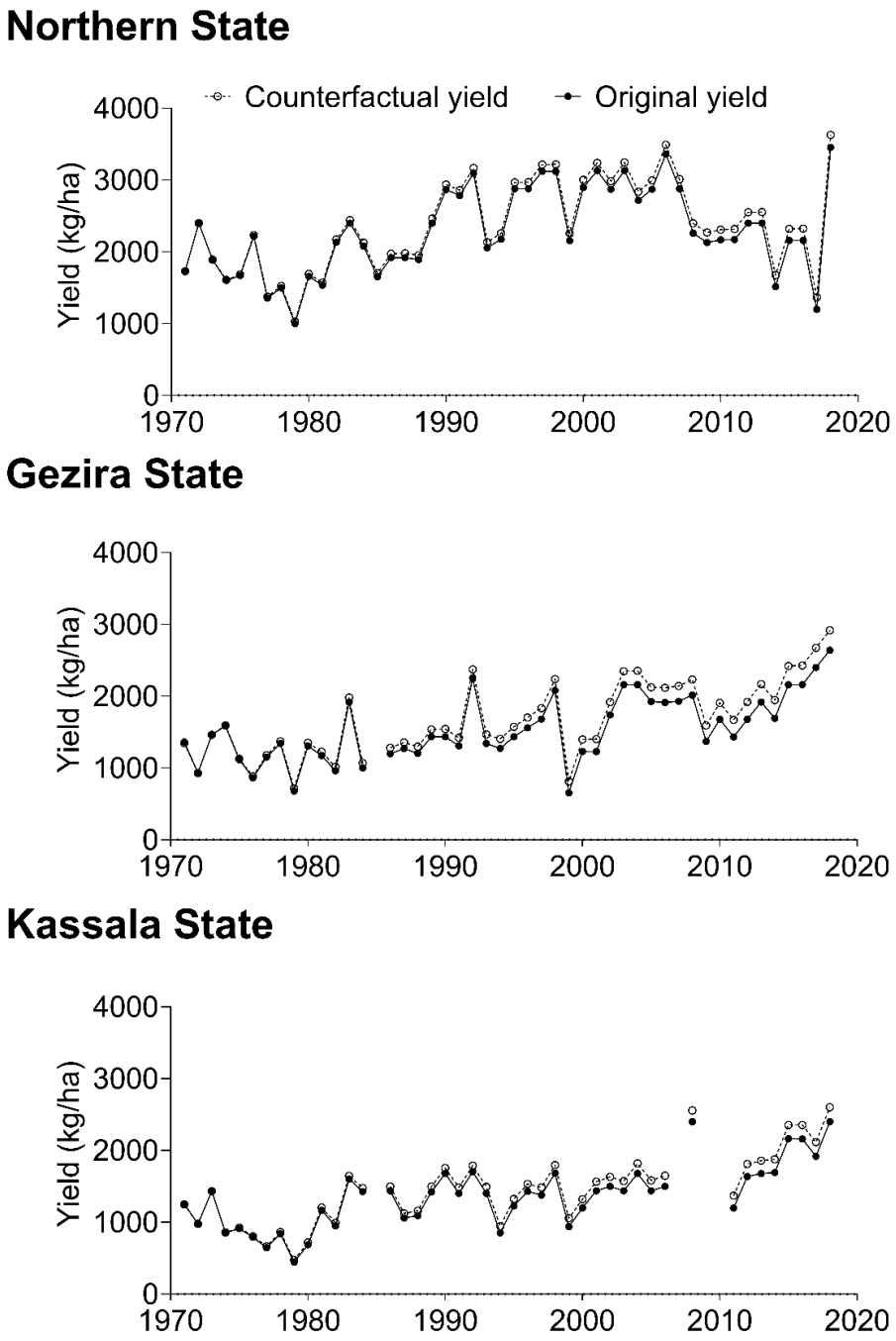

Figure 2.6 Time series (1970/71–2017/18 crop seasons) of the original and counterfactual yields of wheat in Northern State, Gezira State, and Kassala State, Sudan. Counterfactual yield was defined as observed yield minus the effect of increasing temperature. The counterfactual yield is the estimated yield what would occur without increasing temperature over the 48 crop seasons

with growing-season TMAX ($r = -0.43$, $\rho = -0.33$). In Kassala State/New Halfa, yield was negatively correlated with all four indicators, particularly TMIN ($r = -0.55$, $\rho = -0.54$). Relationships of detrended yields with the growing-season TMAX and TMIN are also shown in Figure 2.7. In Gezira State/Wad Medani, yield decreased with increased TMAX from 32.6 °C to 37.1 °C ($p \leq 0.05$). In Kassala State/New Halfa, yield was negatively associated with TMAX between 32.7 °C and 37.2 °C and TMIN between 14.6 °C and 19.1 °C ($p \leq 0.05$).

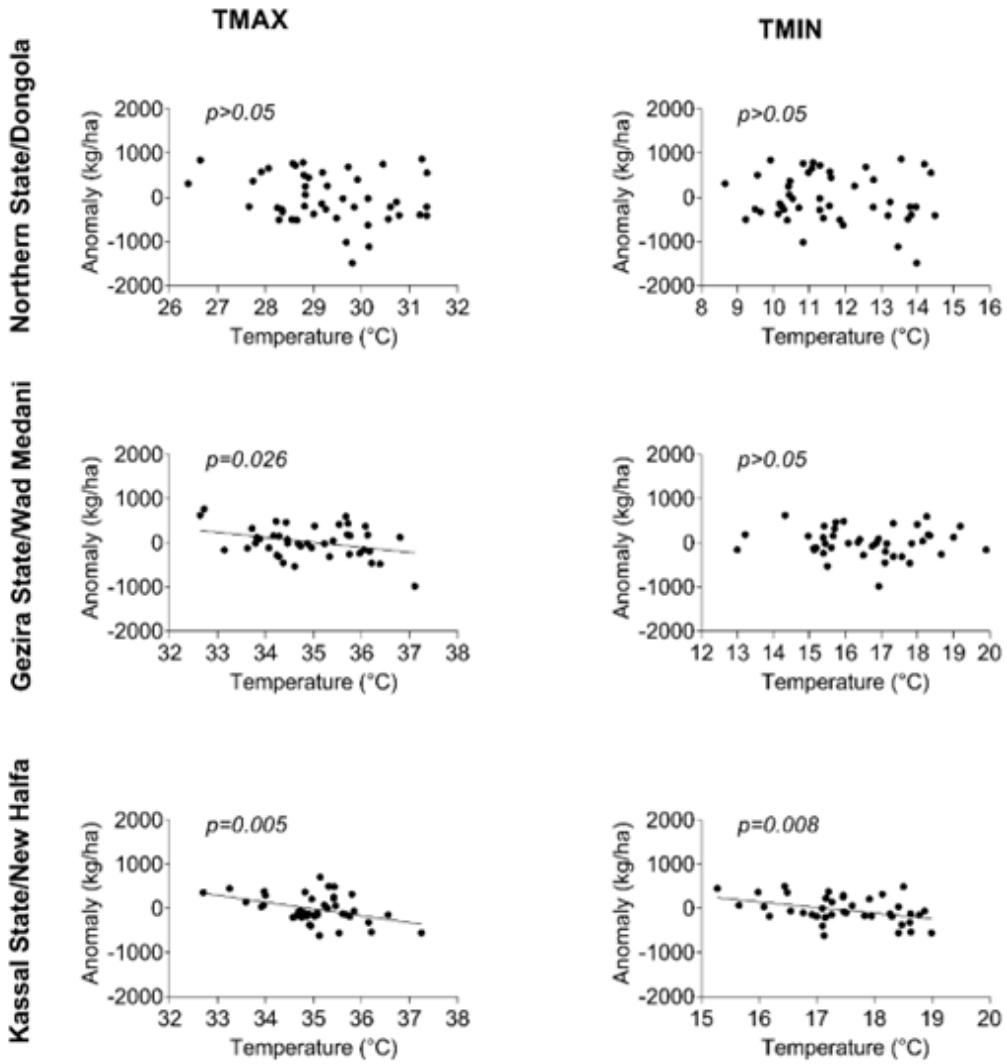

Figure 2.7 Relationships between wheat yield anomalies and growing-season (November-February) average daily maximum (TMAX) and minimum temperatures (TMIN) for Northern State/Dongola, Gezira State/Wad Medani, and Kassala State/New Halfa, Sudan. Linear lines (estimated by least squares regression) in the figures are significant yield–temperature relationships

Table 2.2 Pearson correlation and Spearman's rank correlation between wheat yield anomalies in Northern State, Gezira State, and Kassala State and temperature indicators at the respective meteorological stations (Dongola, Wad Medani, and New Halfa)

Production area/Station	Temperature indicator	November		December		January		February		Season	
		r	ρ	*r*	ρ	*r*	ρ	*r*	ρ	*r*	ρ
Northern State/ Dongola	TMAX	–0.05 ns	–0.05 ns	–0.19 ns	–0.25 ns	–0.10 ns	–0.07 ns	–0.32 *	–0.22 ns	–0.26 ns	–0.26 ns
	TMIN	-0.19 ns	–0.13 ns	–0.04 ns	–0.13 ns	–0.07 ns	–0.04 ns	–0.19 ns	–0.21 ns	–0.17 ns	–0.21 ns
	THD	–0.251 ns	–0.24 ns	0.10 ns	–0.04 ns	–0.16 ns	–0.08 ns	–0.11 ns	–0.20 ns	–0.22 ns	–0.32 *
	THN	–0.38 *	–0.33 *	–0.06 ns	–0.04 ns	–0.11 ns	–0.07 ns	–0.05 ns	–0.15 ns	–0.41 **	–0.38 **
Gezira State/ Wad Medani	TMAX	–0.23 ns	–0.17 ns	–0.18 ns	–0.15 ns	–0.38 **	–0.36 *	–0.28 ns	–0.16 ns	–0.43 **	–0.33 *
	TMIN	-0.11 ns	-0.10 ns	-0.19 ns	-0.10 ns	–0.28 ns	–0.26 ns	0.18 ns	–0.10 ns	–0.15 ns	–0.17 ns
	THD	–0.16 ns	–0.21 ns	–0.19 ns	–0.18 ns	0.09 ns	0.12 ns	0.10 ns	0.11 ns	–0.31 *	–0.19 ns
	THN	–0.06 ns	–0.03 ns	0.07 ns	0.05 ns	–0.04 ns	–0.05 ns	–0.09 ns	–0.14 ns	–0.10 ns	–0.09 ns
Kassala State/ New Halfa	TMAX	–0.32 *	–0.28 ns	–0.23 ns	–0.19 ns	–0.41 **	–0.39 **	–0.23 ns	–0.19 ns	–0.42 **	–0.26 ns
	TMIN	–0.42 **	–0.54 **	–0.27 ns	–0.26 ns	–0.37 *	–0.37 *	–0.26 ns	–0.23 ns	–0.55 **	–0.54 **
	THD	–0.24 ns	–0.31 *	–0.18 ns	–0.15 ns	–0.35 *	–0.31 *	–0.22 ns	–0.22 ns	–0.42 **	–0.30 ns
	THN	–0.32 *	–0.41 **	–0.10 ns	–0.13 ns	–0.04 ns	–0.22 ns	–0.46 **	–0.41 **	–0.41 **	–0.51 **

*TMAX, maximum temperature; TMIN, minimum temperature; THD, proportion of hot days in a month; THN, proportion of hot nights in a month; r, Pearson's correlation coefficient; ρ, Spearman's rank correlation coefficient; *p ≤ 0.05; **p ≤ 0.01; ns, not significant*

2.4. Discussion

The Global Climate Report (NOAA 2020) reveals that 8 of the 10 warmest years at a global scale in the 140-year record have occurred since 2010; in Africa, the 5 warmest years have occurred since 2015, and the increasing trend in annual temperature since 1981 (0.31 °C per decade) has been more than twice that since 1910 (0.12 °C per decade). Our study showed increasing trends in annual TMAX and TMIN for the last five decades in three regions in Sudan (Figure 2.2). This is in line with the study by Elagib and Mansell (2000), who reported increasing trends in annual mean temperature in Sudan from the 1940s to the mid-1990s at a rate of 0.12 °C per decade at Wad Medani and 0.19 °C per decade at the Kassala meteorological station (15.47°N, 36.40°E, 500 m), which is located in the eastern region about 86 km east from New Halfa. Our findings are further supported by a study conducted in the Blue Nile–eastern Sudan region (Xu et al. 2010).
Elagib and Mansell (2000) have reported no trend in annual mean temperature at Dongola, but we found temperature trends increasing at high rates, particularly annual TMIN, indicating that the warming progresses in the northern region of the country. Increasing temperature trends have been reported from neighboring countries. The east and south parts of the Upper Blue Nile River Basin in northwestern Ethiopia, which is adjacent to the eastern region of Sudan, had rising trends in both annual TMIN and TMAX in 1981–2010 at a rate of between 0.1 and 0.15 °C per decade (Mengistu et al. 2014). In East Africa (Kenya, Uganda, and Tanzania), annual temperature increased by 1.5 °C during 1951–2010 (Ongoma and Chen 2017). The highest daily TMAX (close to 50 °C) and TMIN (35 °C) at Dongola and the highest daily TMIN (> 32 °C) at Wad Medani and New Halfa were recorded after 2008. These recorded extremes also indicate that the study areas have been experiencing rapid warming in the last decade.

In the study areas, high temperatures occur late in the hot season (March–May) or early in the wet season (June–October), and therefore, wheat is grown under cooler temperature in the dry season (Figure 2.3). Elagib (2010) has reported that the dry-season TMIN increased at a rate of 0.185 °C per decade at Wad Medani from the 1940s to the mid-2000s, but found no trend in TMAX, whereas we found no trend in TMIN but an increasing trend in TMAX (Figure 2.4). The trend rate of TMIN at New Halfa was, by and large, consistent with the previously reported rate at the Kassala meteorological station (0.357 °C per decade). For Dongola, we found increasing trends in both TMAX and TMIN, and the TMIN rate was more than double the TMAX rate, implying that rapid

warming is occurring in the nighttime during the growing season. In contrast, Elagib (2010) reported no increasing trend in dry-season (October–March) TMAX or TMIN at Dongola and even a decreasing trend in TMAX (− 0.166 °C per decade). This difference might be attributed to a difference in the data analysis between the studies, i.e., different study periods.

The increasing trend rate of yield was around 20 kg/ha per year (Figure 2.5). This confirms the long-term improvement of spring wheat cultivars, which efficiently respond to nitrogen fertilizer, since 1960 (Tahir et al. 2020a). Meanwhile, the difference between the original and counterfactual yields was increasing (Figure 2.6) with increasing temperature (Figure 2.4). To avoid the confounding influence of increasing yield and temperature trends, we used the data detrending approach to analyze the relationship between yield and temperature variations. Consistent with previous reports (e.g., Asseng et al. 2017; Morgounov et al. 2018), we found negative relationships of wheat yields with TMAX and TMIN during the growing season (Table 2.2; Figure 2.7). Loss of pollen viability and shortened grain-filling period decrease grain number and weight, and hence yield (Ishag and Mohamed 1996; Prasad et al. 2008; Nuttall et al. 2018). The best indicator of the growing-season temperature for yield was THN in Northern State/Dongola and TMAX in Gezira State/Wad Medani, whereas all four indicators were significant in Kassala State/New Halfa. These findings imply that THN in northern areas, TMAX in central areas, and all four indicators in eastern areas can be used to detect the effect of high temperature on wheat production. Asseng et al. (2017) reported a negative relationship between yield and mean growing-season temperature in hot environments where spring wheat is grown under irrigated conditions, e.g., in northern India. Such relationships have also been reported for rainfed spring wheat in cool and warm regions in Canada, the USA, Russia, and Kazakhstan (Morgounov et al. 2018). A model simulation study by Lobell et al. (2005) showed the association of increasing yield with decreasing TMIN during 1988–2002 in irrigated wheat production regions of northeast Mexico.

High daytime temperature (≥ 35 °C) during anthesis decreases seed set and grain number (Narayanan et al. 2015; Nuttall et al. 2018). In the central and eastern regions of Sudan, wheat flowers mostly in January, which could partially explain the negative relationship between yield and January TMAX in Gezira State/Wad Medani and Kassala State/New Halfa (Table 2.2). In crop modeling, the negative effect of daily TMAX on wheat yield is demonstrated by setting an upper

temperature limit (e.g., 34 °C in APSIM) for calculating a heat-stress factor (Asseng et al. 2011). Here, 35 °C was set as the threshold temperature to calculate THD, but no specific monthly THD had a negative effect on yield, although Kassala State/New Halfa had a weak correlation of yield with November THD. The optimum temperature for wheat is around 20 °C (Porter and Gawith 1999); therefore, daily TMIN should be below 20 °C. In this study, 20 °C was set as the threshold to calculate THN. Monthly minimum temperature indicators (THN and TMIN) in January and February (heading, flowering, and ripening period in central and eastern Sudan) had a negative effect on yield in Kassala State/New Halfa (Table 2.2). This is in line with the negative effect of the nighttime temperature ≥ 20 °C during grain filling on wheat grain number per spike and size (Prasad et al. 2008), and during anthesis on grain number and grain yield (Narayanan et al. 2015). In crop modeling, both the upper limit for daily TMAX and that for daily TMIN can be crucial for simulating the effect of high temperature on wheat yield in Sudan.

Crop yield can be influenced by government policies such as socioeconomic transformation of agricultural industry (e.g., Hlavinka et al. 2009) and economic liberalization (e.g., Al-Feel and AL-Basheer 2012). In Northern State, the sharp dropped yield in the 2007/08 season (Figure 2.5) might have happened because the government stopped support for agricultural inputs in wheat production in the mid-2000s, and accordingly the farmers might have minimized the use of the inputs such as fertilizers.

2.5. Conclusions

The yield–temperature relationship analysis is needed to understand wheat production in hot environments under changing climate. Using trend analyses of temperature indicators and wheat yields, we showed upward trends in both the annual and growing-season temperatures. In particular, nighttime temperature in the northern region (Dongola) is rapidly raising. The yields are negatively associated with both daytime and nighttime temperature indicators during the growing season, and the negative effect of raising temperature on yield has increased in recent years. Specifically, the yield deviation is associated with THN in the northern region, TMAX and THD in the central region, and TMAX, TMIN, THD, and THN in the eastern region. In the central and eastern regions, the temperature indicators in January (during the heading to flowering period) contribute the most to the yield deviation. Thus, Sudan is likely warming, which will adversely affect the country's

breadbasket in coming decades.

Chapter 3
Dynamical Downscaling of Climate Variables

3.1. Introduction

Previous studies have tested various physical options of the WRF model to identify the most suitable configurations for specific regions. For example, over the Middle East and North Africa (MENA), the climates of which are hot and dry, rainfall is sensitive mainly to cumulus parameterization physics such as the Kain–Fritsch scheme (KF) (Kain 2004), the Grell–Devenyi ensemble scheme (GD) (Grell and Dévényi 2002) and the Betts–Miller–Janjic scheme (BMJ) (Janjić 1994), whereas microphysics such as the Goddard scheme (GODDARD) (Tao et al. 1989) and the WRF Single-moment 6-class scheme (WSM6) (Hong and Lim 2006) significantly affect temperature deviations (Zittis et al. 2014). However, the model outputs are less sensitive to planetary boundary layer physics, such as the Mellor–Yamada–Janjic scheme (MYJ) (Janjić 1994) and the Yonsei University scheme (YSU) (Hong et al. 2006), than to cumulus parameterization physics and microphysics (Zittis et al. 2014a). In the case of shortwave and longwave radiation physics, the Community Atmosphere Model (CAM) (Collins et al. 2006) and Rapid Radiative Transfer Model for GCMs (RRTMG (Iacono et al. 2008) capture well the inter-annual variability and warming trends of temperature, but they are season- and location-dependent over MENA (Zittis and Hadjinicolaou 2017a). A previous study (Constantinidou et al. 2020) has further indicated that temperature is sensitive to land surface physics such as the Noah land surface model (NOAH) (Mitchell et al. 2005), NOAH with multi-parameterization (NOAHMP) (Niu et al. 2011), Community Land Model (CLM) (Bonan 1996), and the Rapid Update Cycle (RUC) (Smirnova et al. 1997). The following configuration of the WRF model has been recommended for MENA: CAM or RRTMG, NOAH, YSU, the WRF Single-moment 5-class scheme for microphysics (WSM5) or WSM6, and KF (Zittis et al. 2014; Zittis and Hadjinicolaou 2017b; Constantinidou et al. 2020).

The sensitivity of the WRF model outputs to the physics options has been reported for the neighboring regions of MENA, i.e., the Nile River basin and the Eastern Nile basin. The configuration recommended for the Nile River basin is a combination of the Dudhia scheme for shortwave radiation (DUDHIA) (Dudhia 1989) and the Rapid Radiative Transfer Model for

longwave radiation (RRTM) (Mlawer et al. 1997), NOAH, MYJ, the WRF Single-moment 3-class scheme for microphysics (WSM3) (Hong et al. 2004), and KF (Tariku and Gan 2018). For the Eastern Nile basin, the climates of which are wetter than those of MENA, a set of CAM, NOAH, MYJ, WSM6, and BMJ is recommended (Abdelwares et al. 2018). In the case of rainfall, the WRF model outputs are very sensitive to the cumulus parameterization option (Zittis et al. 2014; Tariku and Gan 2018; Abdelwares et al. 2018; Ratna et al. 2014; Igri et al. 2018; Otieno et al. 2020). There are two types of cumulus parameterization options: adjustment and mass-flux. The BMJ is a typical adjustment type, whereas the GD and KF are examples of the widely used mass-flux type. The WRF model with the adjustment type does not simulate detailed processes of cumulus convection. Instead, it uses a simplified process that involves adjusting lapse rates of temperature and humidity. Compared with the adjustment type, the mass-flux type is complex because it involves cloud modelling for cumulus convective processes. The model performance with this type depends mainly on the reproduction of entrainment/detrainment and/or updrafts/downdrafts. The performance of WRF downscaling experiments has been reported from different regions of Africa. For example, the BMJ outperforms the GD in South Africa (Ratna et al. 2014), where it reproduces the intensity of summer rainfall anomalies, and the KF and GD over Central and Western Africa (Igri et al. 2018). Over East Africa, model simulation with the KT incorporating a moisture-advection-based trigger function (KFT) as well as the KT and GD (Ma and Tan 2009) outperforms model simulation with the BMJ (Otieno et al. 2020).

In Northeast Africa, drought and extremely high temperature events often occur and negatively affect crop production. Sudan is one of the countries vulnerable to such climate risks: droughts impact summer crops such as sorghum and pearl millet during the wet season from June to September in the relatively wet climate of the southern part (Elagib 2013), and high temperatures affect irrigated wheat during the dry season from November to February in the dry climate of the central and northern parts (Musa et al. 2021). Rainfall is a critical climate element in the wet season because summer crops are cultivated under rainfed conditions. Lack of rain results in crop failure, hence the economic loss. In the dry season, wheat is produced under irrigated conditions due to no rain falling in the cultivated areas, but the crop is often exposed to heat stress. Previous studies have shown that yields of the summer crops are positively associated with rainfall in the wet season (Elagib 2013), and irrigated wheat yield is negatively associated with temperature in the dry season

(Musa et al. 2021). The main objective of this study was therefore to identify a robust configuration of the WRF model for generating high-spatial-resolution climate data for crop growing seasons in Sudan. The focus was on wet season rainfall and dry season temperature. The specific objectives were (1) to compare downscaled rainfall and temperature data between cumulus parameterization schemes and (2) to determine cumulus parameterization schemes for specific growing seasons and climatic zones.

3.2. Methods

3.2.1. Study area

Sudan is one of the most water-scarce countries in the world. Based on the aridity index (Middleton and Thomas 1992), the Sudan can be divided into three aridity zones, hyper-arid, arid, and semi-arid. These zones are all characterized by hot, wet summers and relatively cold, dry winters. In general, northern Sudan receives less rainfall and experiences larger temperature changes between seasons than southern Sudan. For example, Dongola (19.17° N, 30.48° E) receives less than 15 mm of annual rainfall, and the range of monthly mean temperatures is 17.6–34.5 °C; the annual rainfall at Wad Medani (14.40° N, 33.48° E) is about 300 mm, and the range of monthly mean temperatures is 23.6–33.1 °C; at Gedaref (14.03° N, 35.40° E), the annual rainfall is about 600 mm, and the range of monthly mean temperatures is 25.9–32.7 °C. These sites are in the hyper-arid, arid, and semi-arid zones, respectively (Elagib and Mansell 2000). The topography of Sudan is relatively flat, except in the southwestern part (Figure 3.1).

3.2.2. Model configuration

We used the WRF model version 4.2 (Advanced Research WRF). The BMJ scheme has been commonly selected in WRF downscaling experiments in the Nile River basin and the Eastern Nile basin (Abdelwares et al. 2018; Tariku and Gan 2018). The KFT scheme, the Tiedtke scheme (Tiedtke 1989), and the Grell–Freitas scheme (GF) (Grell and Freitas 2014) perform well to some extent in the neighboring regions of Sudan, i.e., East Africa (Mugume et al. 2017; Otieno et al. 2020) and West Africa (Adeniyi 2019). However, to the best of our knowledge, the KFT, Tiedtke, and GF are never tested in the study area. Therefore, the following schemes were selected to evaluate the sensitivity of model outputs to cumulus parameterization: (a) BMJ (Janjić 1994), an adjustment type of the convection scheme introduced by Betts and Miller (1986); (b) KFT (Ma

and Tan 2009), an improved mass-flux scheme of Kain and Fritsch (1993) based on Fritsch and Chappell (1980) for a convective system of detrainment from clouds; (c) a modified Tiedtke (TDK) scheme (Zhang et al. 2011), a modification of the mass-flux scheme of Tiedtke (1989) with respect to entrainment and detrainment in cumulus convection; and (d) GF (Grell and Freitas 2014), a mass-flux scheme with the stochastic approach of Grell and Dévényi (2002) based on Grell's original scheme (Grell 1993). The other four physics schemes selected for this study were the RRTMG, unified NOAH (Mukul Tewari et al. 2004), YSU, and WSM6 for shortwave and longwave radiation physics, land surface physics, planetary boundary layer physics, and microphysics, respectively. These were chosen based on recommendations found in previous studies of Northeast Africa (Zittis et al. 2014; Zittis and Hadjinicolaou 2017b; Abdelwares et al. 2018; Tariku and Gan 2018; Constantinidou et al. 2020; Otieno et al. 2020).

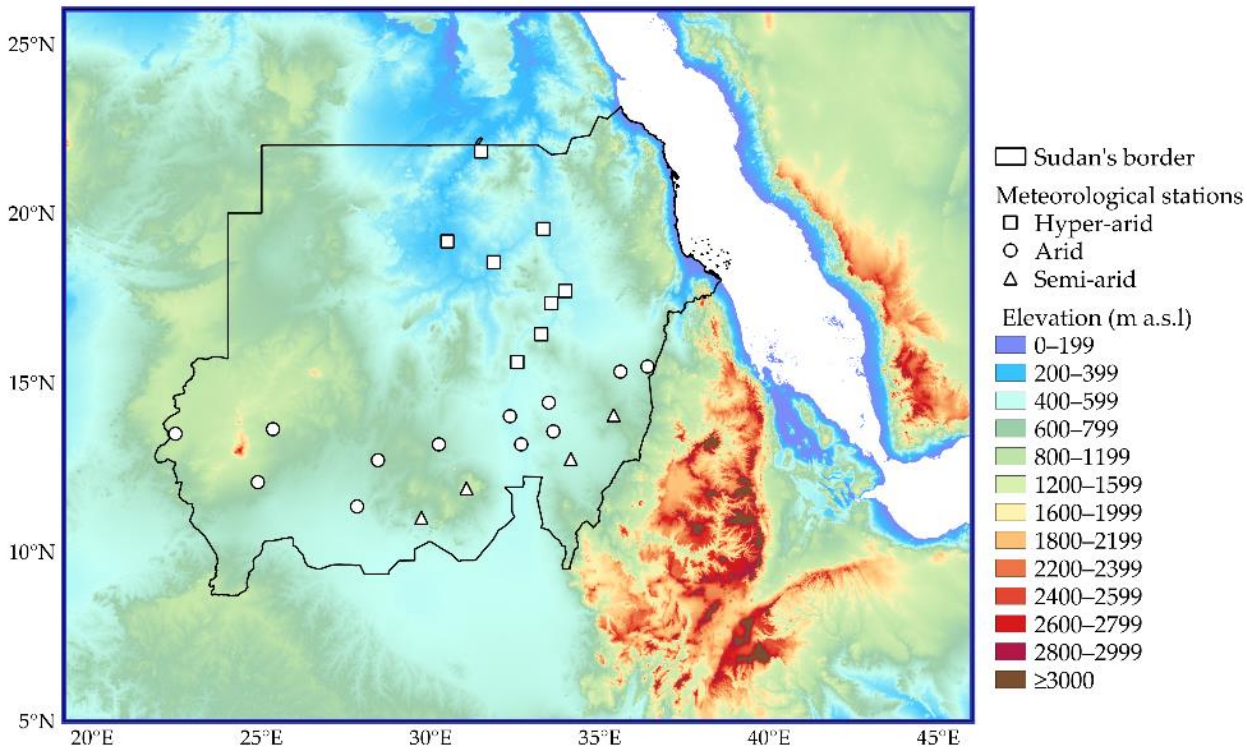

Figure 3.1 The domain of the Weather Research and Forecasting downscaling experiment with geographical locations of 24 meteorological stations in the hyper-arid, arid, and semi-arid zones of Sudan.

3.2.3. Model simulation

A set of experiments was run to test these cumulus parameterization schemes using 6-hourly data from the National Centers for Environmental Prediction (NCEP-Climate Forecast System Reanalysis (CFSR)) at a horizontal resolution of 0.5° × 0.5° (Saha et al. 2010). The NCEP-CFSR dataset is available for the period 1979–2010 from the Research Data Archive of Computational and Information Systems Laboratory of the National Center for Atmospheric Research (ds093.0) (https://rda.ucar.edu) (accessed on 19 March 2021). In this study, the downscaling experiments were carried out for 10 years from 2000 to 2010 by running the model from May of each year to May of the following year. The NCEP-CFSR data were downscaled to 10 km horizontal resolution for a single domain centered over Sudan (Figure 3.1) using the WRF Preprocessing System version 4 consisting of the 10 min surface topography data (slope category, terrain height, soil type, soil temperature) of the United States Geological Survey and the land use data (albedo, vegetation fraction, land use classification,) of the Moderate Resolution Imaging Spectroradiometer (MODIS (https://www2.mmm.ucar.edu/wrf/users/download/get_sources_wps_geog.html) (accessed on 20 November 2020).

3.2.4. Model validation

Daily rainfall data and maximum and minimum temperatures (TMAX and TMIN, respectively) at 24 meteorological stations (Figure 3.1) were obtained from the Sudan Meteorological Authority. Annual, seasonal, and monthly averages of daily rainfall, TMAX, and TMIN were used to evaluate model performance. For seasonal and monthly comparisons, wet season (June–September) and dry season (November–February) data were used for rainfall and temperature, respectively. TMAX was also used for the comparisons for the wet season in relation to heat stress to crops. Moreover, the number of rainy days (NRD) (daily rainfall ≥ 1 mm) in the wet season and the frequency of hot days (FHD) (daily TMAX > 35 °C) in the dry season were used as drought and extreme temperature indices, respectively.

Model validation was performed using the data averaged over the meteorological stations located in each climatic zone. For statistical analysis of the downscaling experiments, a Taylor Diagram was used to depict the similarity between the experimental outputs and the corresponding observed data (10 years). The diagram showed the Pearson correlation coefficient (R), standard deviation

(SD), and root-mean-square error (RMSE) (Taylor 2001). The significance of the correlation coefficient was tested at $p \leq 0.05$ (2-tailed). We normalized both the SD of the simulated data and the RMSE to the SD of the observed data. The spatial distributions of the simulated rainfall and temperature data were also compared with the 10-year average satellite-based reanalysis data, i.e., the Integrated Multi-Satellite Retrievals for GPM (IMERG) (Huffman et al. 2020) (https://gpm.nasa.gov) (accessed on 17 May 2021) for rainfall at a horizontal resolution of 0.1° × 0.1° and the Modern-Era Retrospective analysis for Research and Applications, Version 2 (MERRA2) (Celaro et al. 2017) (https://gmao.gsfc.nasa.gov) (accessed on 26 April 2021) for temperature at a horizontal resolution of 0.5° × 0.625°. The IMERG database has been developed since 2000, using the data collected with the TRMM/GPM onboard Dual-frequency Precipitation Radar and Microwave Imager together with other passive microwave radiometers such as GCOM-W1 AMSR2 and NOAA-20 ATMS. The MERRA2 dataset (1980 to present) has been generated on a cubed-sphere grid with the GEOS General Circulation Model.

3.3. Results

3.3.1. Annual rainfall and temperature

Figure 3.2a shows the spatial distribution of annual rainfall. The simulated data and the satellite-based data were comparable in the central to northern part of the study area. The rainfall simulated with the BMJ scheme most closely agreed with the satellite-based data (IMERG) (Figure 3.2a, Table 3.1). Use of the KFT and GF schemes resulted in slight overestimates of rainfall in southern Sudan, and the rainfall simulated by the TDK was low in northern Sudan. In southeastern Sudan, the KFT-simulated rainfall was more-or-less in agreement with the satellite-based data. All four schemes produced results that were very strongly correlated with the satellite-based data ($R = 0.92$ for BMJ, 0.96 for KFT, 0.93 for TDK, 0.97 for GF). The normalized SD for the BMJ scheme was close to unity. The BMJ scheme had the lowest RMSE, followed by the TDK and then the KFT scheme (Table 3.1). Figure 3.2b shows the spatial distribution of the annual TMAX. The distributions simulated with the BMJ, KFT, and TDK schemes were comparable with the MERRA2 data, except in the northeastern corner of Sudan, whereas the GF reproduced the low TMAX in the central to southern and central to eastern parts of the Sudan. All four schemes simulated temperatures that were strongly correlated with the satellite-based data, and the normalized SD was close to unity (Table 3.1). The RMSEs of the temperatures simulated by the

KFT and TDK were lower than the corresponding RMSEs of the BMJ and GF. Like TMAX, the simulated TMIN was strongly correlated with the satellite-based data, and the normalized SD was close to unity (Table 3.1). However, the RMSE was higher Atmosphere for TMIN than for TMAX in all four schemes. The simulated TMIN was higher than the satellite-based TMIN over the study area (Figure 3.2c).

3.3.2. Wet season rainfall and temperature

Figure 3.3a shows the spatial distribution of the wet season (June–September) rainfall. Like annual rainfall, the wet season rainfall simulated with the BMJ scheme was highly consistent with the IMERG data. The wet season rainfall simulated by all four schemes was very strongly correlated with the satellite-based rainfall (R = 0.91 for BMJ, 0.96 for KFT, 0.92 for TDK, 0.97 for GF). The RMSE of the wet season rainfall simulated by the BMJ was the lowest among the schemes. The variance of the BMJ rainfall was low, and its normalized SD was close to unity (Table 3.1). Figure 3.4 shows Taylor diagrams of monthly and seasonal rainfall to allow comparisons between climatic zones. The seasonal rainfall simulated by all the schemes was significantly correlated with observed seasonal rainfall in the hyper-arid zone (R = 0.94 for BMJ, 0.85 for KFT, 0.93 for TDK, 0.96 for GF). The simulated NRD also agreed with the observed data for TDK (R = 0.81) and GF (R = 0.68) (Table 3.2). The simulated monthly rainfall was also in agreement with the observed rainfall in June and July, and the GF-simulated rainfall was significantly correlated with the observed rainfall in August (Figure 3.4). In all months, both the SD and RMSE were higher for the GF-simulated rainfall than for the other schemes. In the arid zone, correlations were high between the seasonal rainfall simulated with the BMJ and GF schemes and the observed rainfall. The BMJ-simulated NRD was also consistent with the observed data (R = 0.64), but no correlation was found between GF-simulated and observed NRDs (Table 3.2). There were significant correlations between observed and simulated monthly rainfall for all four schemes in July and September, except for the TDK in July, but there were no analogous correlations in June and August (Figure 3.4). In general, the SD and RMSE were lower for the BMJ- and TDK-simulated rainfall than for the KFT- and GF-simulated rainfall. In the semi-arid zone, no correlations were found between simulated and observed seasonal rainfall, but KFT-simulated monthly rainfall was significantly correlated with observed rainfall in July and August. The BMJ- and GF-simulated rainfalls were consistent with the observed rainfall in July. In addition, the TDK-simulated NRD was

significantly correlated with the observed data (R = 0.71) (Table 3.2). The SD and RMSE of the simulated rainfall were relatively high in the semi-arid zone compared with the hyper-arid and arid zones (Figure 3.4).

The seasonal TMAX simulated by all four schemes was very strongly correlated with the observed data in the hyper-arid zone (R > 0.8) (Table 3.2). In the arid and semi-arid zones, the simulated TMAX was also significantly correlated with the observed data.

Table 3.1 The Pearson correlation coefficient (R), normalized standard deviation (SD), root-mean-square error (RMSE) and normalized RMSE for spatial distributions of annual and seasonal rainfall, maximum temperature (TMAX), and minimum temperature (TMIN). All correlation coefficients are significant at $p \leq 0.01$.

		Annual			**Seasonal**		
Scheme	**Statistics**	**Rainfall**	**TMAX**	**TMIN**	**Rainfall**	**TMAX**	**TMIN**
BMJ	*R*	0.92	0.76	0.88	0.91	0.93	0.94
	Normalized *SD*	0.92	1.04	0.98	0.94	0.98	0.97
	RMSE	113 mm	1.75°C	2.81°C	103 mm	1.80°C	3.20°C
	Normalized *RMSE*	0.42	0.91	1.17	0.44	0.43	0.84
KFT	*R*	0.96	0.76	0.87	0.96	0.91	0.93
	Normalized *SD*	1.53	0.98	0.98	1.46	0.71	0.84
	RMSE	194 mm	1.59°C	2.70°C	141 mm	2.17°C	1.91°C
	Normalized *RMSE*	0.72	0.83	1.13	0.61	0.52	1.24
TDK	*R*	0.93	0.76	0.85	0.92	0.94	0.94
	Normalized *SD*	0.71	1.07	1.12	0.76	0.96	1.03
	RMSE	160 mm	1.58°C	2.67°C	132 mm	1.54°C	3.43°C
	Normalized *RMSE*	0.59	0.82	1.12	0.57	0.37	0.84
GF	*R*	0.97	0.76	0.88	0.97	0.93	0.94
	Normalized *SD*	1.89	0.88	0.83	1.88	0.88	0.91
	RMSE	336 mm	2.10°C	2.72°C	279 mm	1.84°C	3.03°C
	Normalized *RMSE*	1.24	1.10	1.14	1.20	0.44	0.86

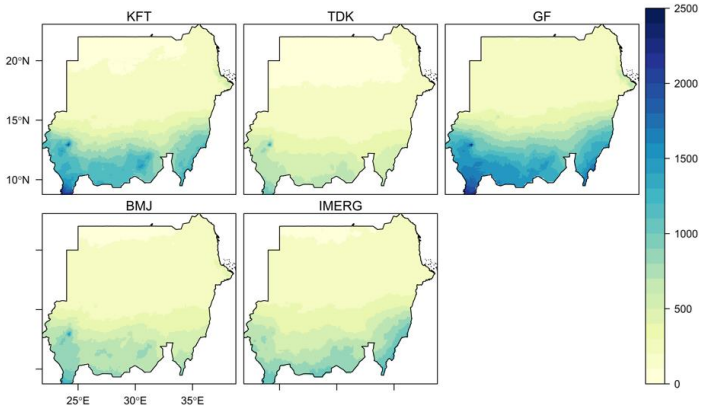

(**a**) Rainfall

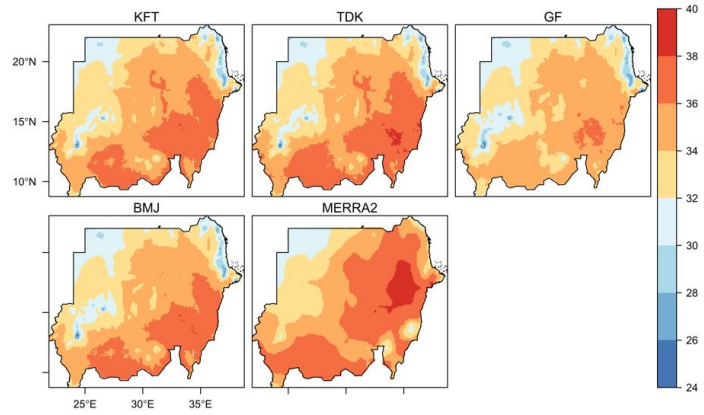

(**b**) Maximum temperature

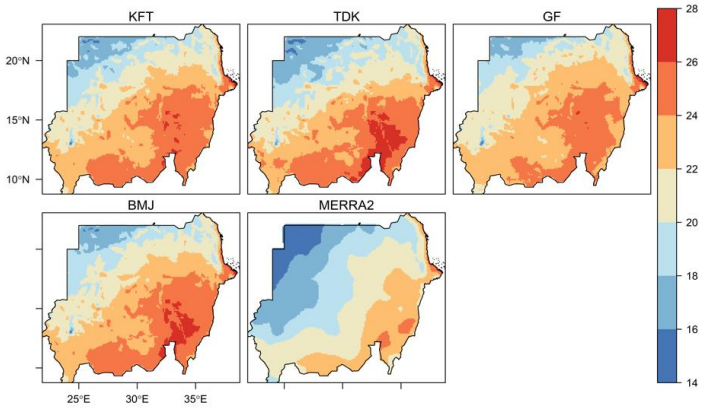

(**c**) Minimum temperature

Figure 3.2 Spatial distributions of the 10-year average annual rainfall (mm) and maximum and minimum temperatures (°C) simulated with the Betts–Miller–Janjic (BMJ), improved Kain–Fritch (KFT), modified Tiedtke (TDK), and Grell–Freitas (GF) schemes, and IMERG observed rainfall data and MERRA2 observed temperature data in Sudan. (a) Rainfall. (b) Maximum temperature. (c) Minimum temperature.

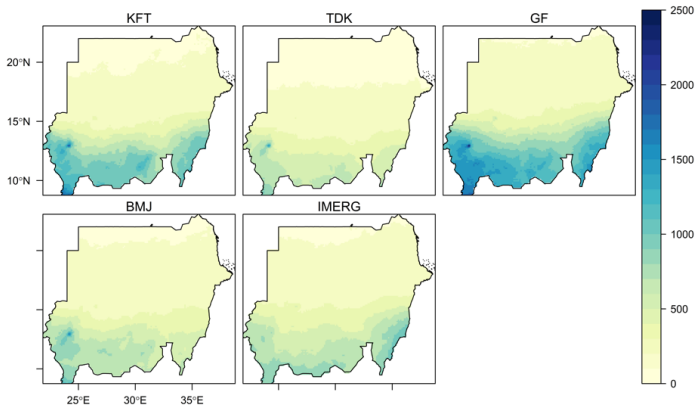

(**a**) Rainfall

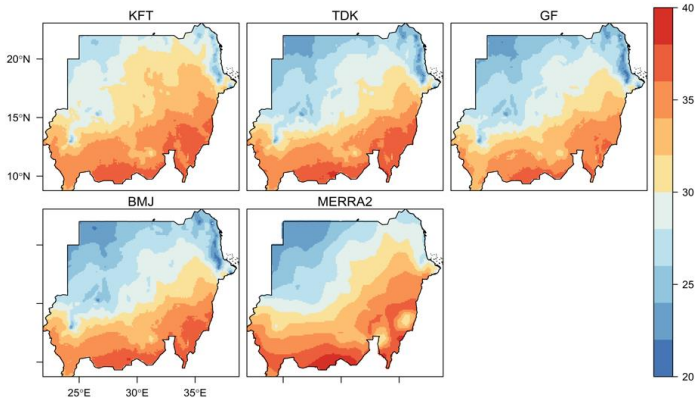

(**b**) Maximum temperature

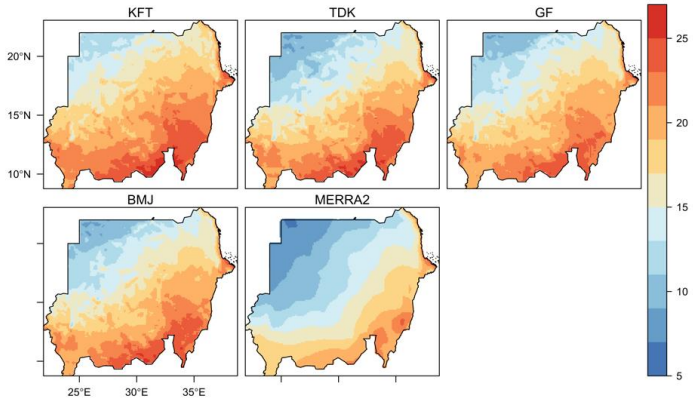

(**c**) Minimum temperature

Figure 3.3 Spatial distributions of the 10-year seasonal (June–September) rainfall (mm) and seasonal (November–February) maximum and minimum temperatures (°C) simulated with the Betts–Miller–Janjic (BMJ), improved Kain–Fritch (KFT), modified Tiedtke (TDK), and Grell–Freitas (GF) schemes, and IMERG observed rainfall data and MERRA2 observed temperature data in Sudan.

3.3.3. Dry season maximum temperature

Figure 3.3b shows the spatial distribution of the dry season (November–February) TMAX. The distributions simulated with the BMJ, TDK, and GF schemes were comparable to that of the MERRA2 data. The KFT-simulated TMAX values were relatively high, particularly in northwestern Sudan, and its RMSEs were higher than those of the other schemes (Table 3.1). The seasonal TMAX values were more highly correlated than the annual TMAX values with the MERRA2 data (R = 0.93 for BMJ, 0.91 for KFT, 0.94 for TDK, 0.93 for GF). The Taylor diagrams further showed that the simulated TMAX agreed with the observed data, except for KFT, in all three zones (Figure 3.5). Similarly, the FHDs simulated by all four schemes were strongly correlated with the observed data in all three zones (Table 3.2). The normalized SDs for BMJ and TDK were close to unity. The RMSEs were higher for the KFT and GF than for the BMJ and TDK schemes. The simulated monthly TMAX was significantly correlated with the observed data, except for the following schemes and months: KFT for December and January, TDK for November, and GF for November and January in the hyper-arid zone; KFT for January and GF for November and January in the arid zone; and BJM and TDK for November and KFT and GF for January in the semi-arid zone.

3.3.4. Dry season minimum temperature

Figure 3.3c shows the spatial distribution of the dry season TMIN. Like TMAX, the spatial distributions of the TMINs simulated with the BMJ, TDK, and GF schemes were comparable to those of the MERRA2 data, but the TMINs simulated by the KFT scheme were relatively high. The TMINs simulated by all four schemes were strongly correlated with the reanalysis data (MERRA2) (R = 0.94 for BMJ, 0.93 for KFT, 0.94 for TDK, 0.94 for GF), and the normalized SDs were near unity (Table 3.1). In contrast to the TMAX values, the RMSEs were relatively high, except for KFT. The Taylor diagrams also showed that the BMJ- and TDK-simulated seasonal TMINs were in agreement with the observed data in all three zones (Figure 3.6). However, the GF-simulated TMINs were not correlated with the observed data in the hyper-arid zone, and the KFT-simulated TMINs were correlated with the observed data only in the arid zone.

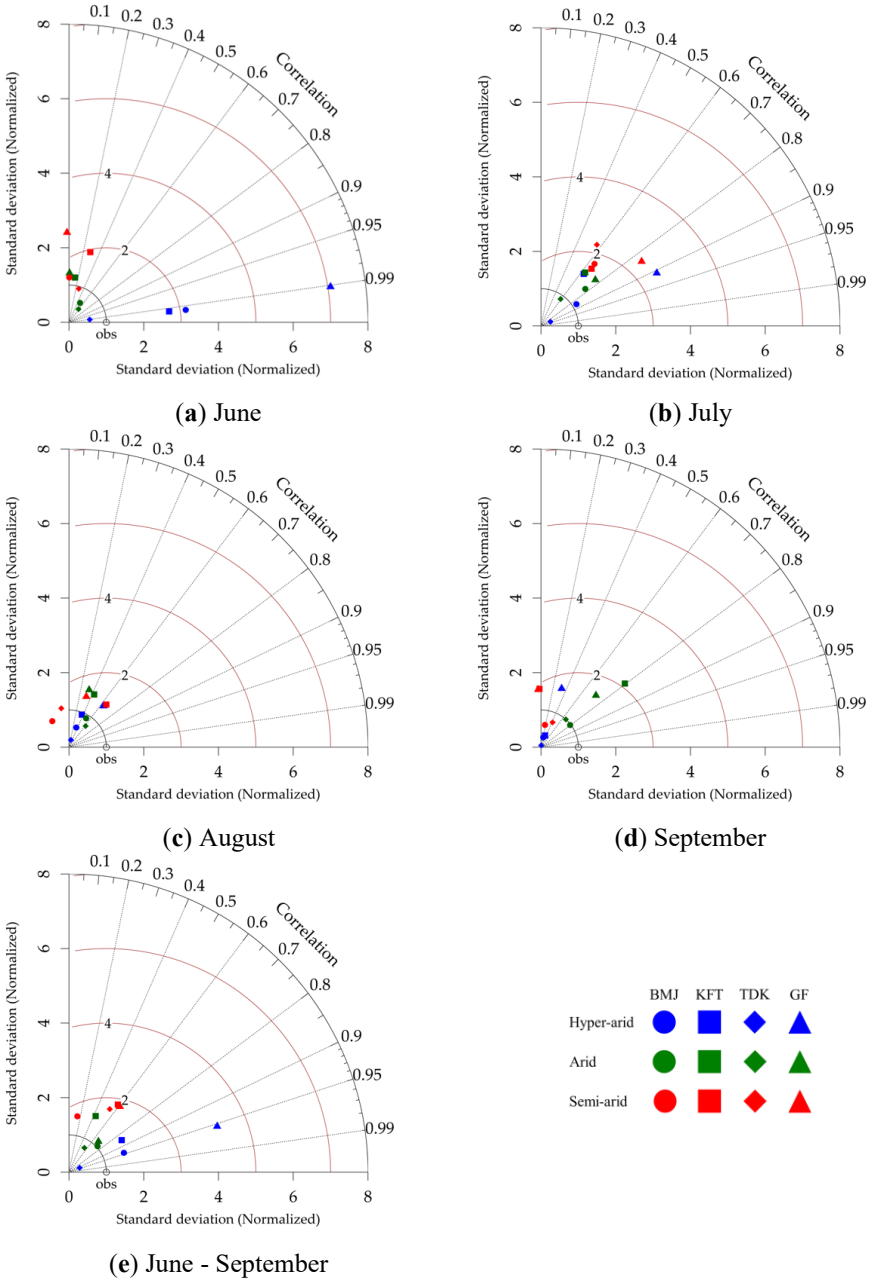

Figure 3.4 Normalized Taylor diagrams (obs: normalized standard deviation of observations) for monthly and seasonal rainfall during the wet season (June–September) in the hyper-arid, arid, and semi-arid zones of Sudan. BMJ, KFT, TDK, and GF are the Betts–Miller–Janjic, improved Kain–Fritch, modified Tiedtke, and Grell–Freitas schemes, respectively. (a) June. (b) July. (c) August. (d) September. (e) June–September

The RMSEs associated with the seasonal TMIN data were relatively high compared to the RMSEs of the TMAX data. The normalized SDs were close to unity in the arid zone but lower than unity in the hyper-arid and semi-arid zones. The monthly TMINs simulated by all four schemes were in agreement with the observed TMIN in February in all three zones, December in the hyper-arid zone, and November in the arid zone. In addition, the TMINs simulated with the following schemes and months were significantly correlated with the observed TMINs in the arid and semi-arid zones: BMJ in December, TDK in November and December, and GF in December and January.

Table 3.2 The Pearson correlation coefficient (R) for seasonal maximum temperature (TMAX) and the number of rainy days (NRD) (daily rainfall ≥ 1 mm) in the wet season (June–September), and the frequency of hot days (FHD) (daily TMAX > 35 °C) in the dry season (November–February). All correlation coefficients are significant at $p \leq 0.05$, and ns denotes no significance.

		Wet Season		**Dry Season**
Zone	**Scheme**	**TMAX**	**NRD**	**FHD**
Hyper-arid	BMJ	0.85	ns	0.82
	KFT	0.81	ns	0.74
	TDK	0.89	0.81	0.85
	GF	0.87	0.68	0.80
Arid	BMJ	0.79	0.64	0.96
	KFT	0.74	0.65	0.90
	TDK	0.84	ns	0.91
	GF	0.89	ns	0.92
Semi-arid	BMJ	0.69	ns	0.95
	KFT	0.80	ns	0.88
	TDK	0.71	0.71	0.94
	GF	0.90	ns	0.87

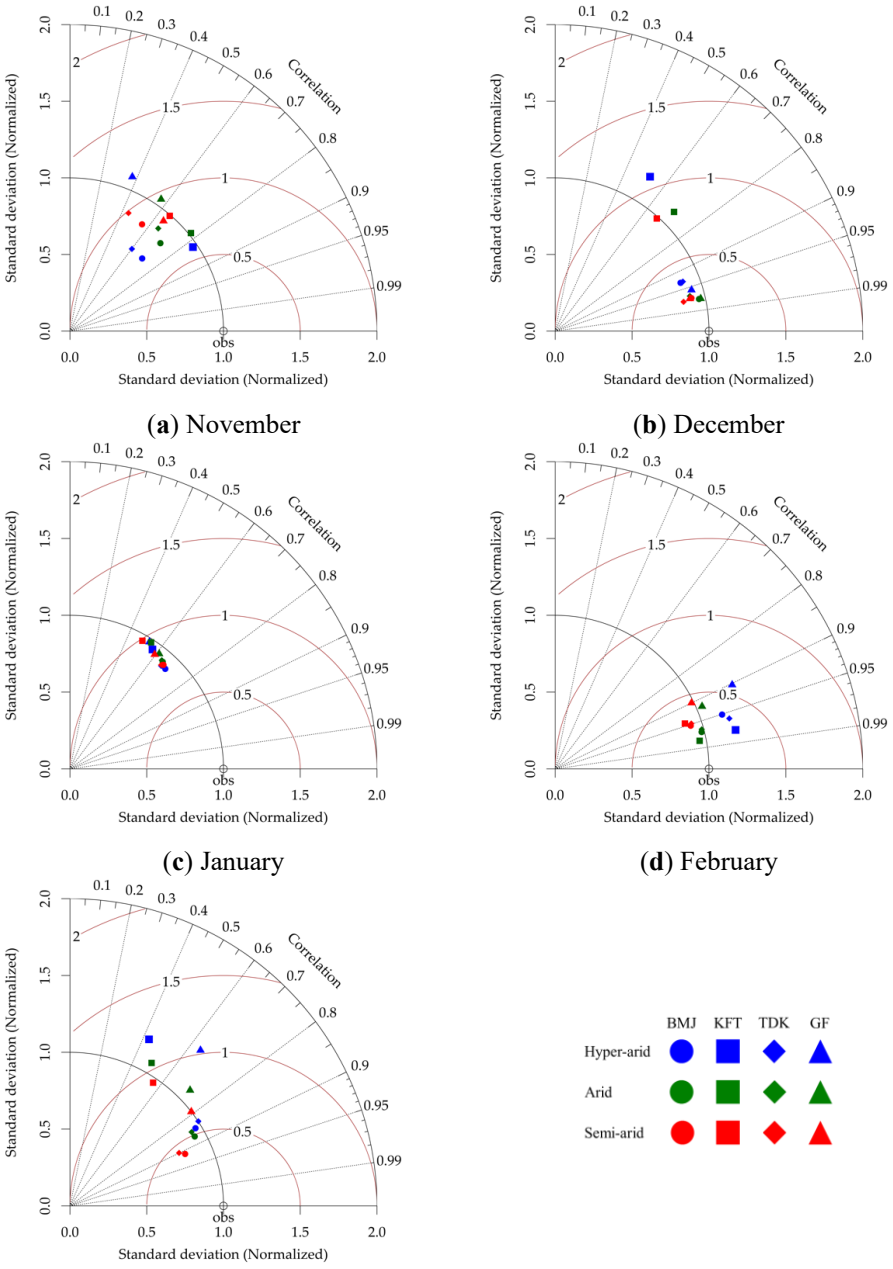

Figure 3.5 Normalized Taylor diagrams (obs: normalized standard deviation of observations) for monthly and seasonal maximum temperature during the dry season (November–February) in the hyper-arid, arid, and semi-arid zones of Sudan. BMJ, KFT, TDK, and GF are the Betts–Miller–Janjic, improved Kain–Fritch, modified Tiedtke, and Grell–Freitas schemes, respectively. (a) November. (b) December. (c) January. (d) February. (e) November–February

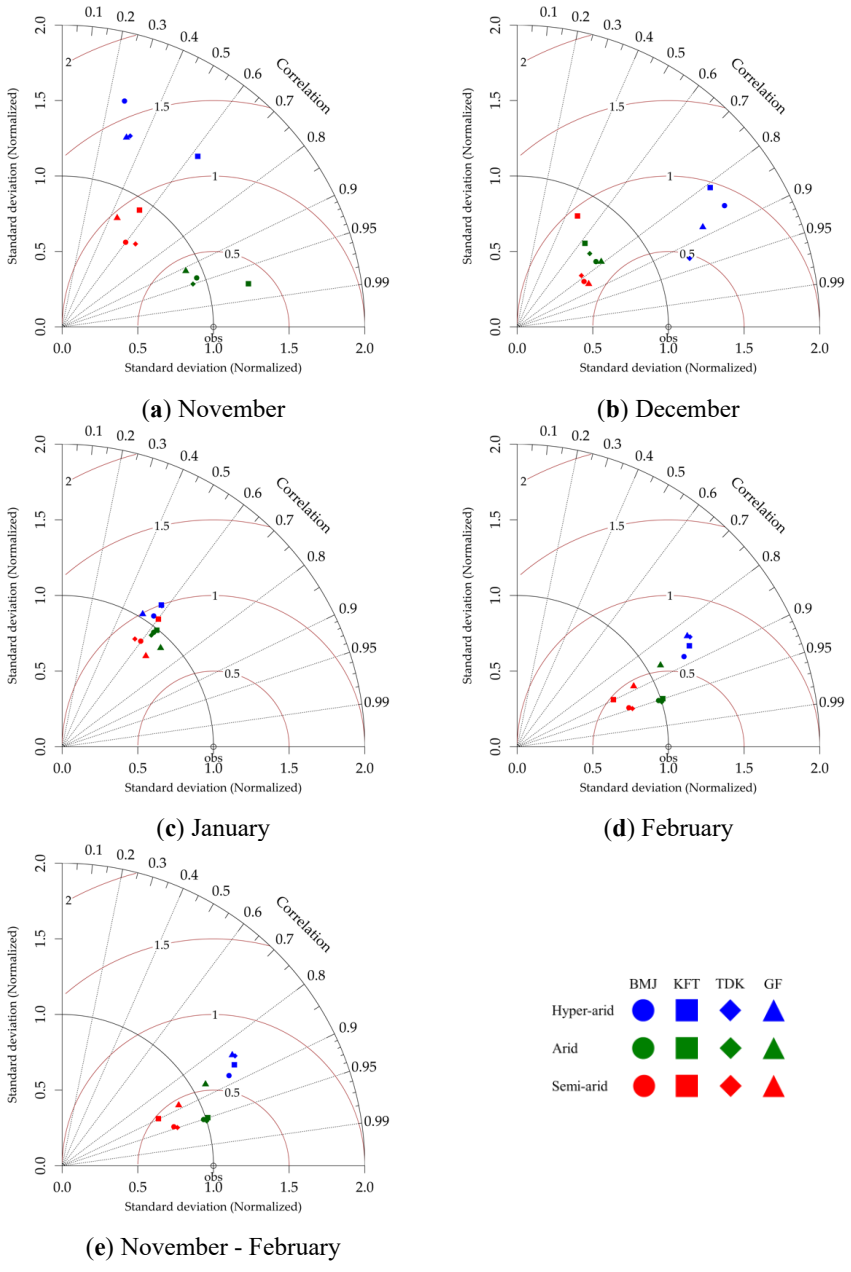

Figure 3.6 Normalized Taylor diagrams (obs: normalized standard deviation of observations) for monthly and seasonal minimum temperature during the dry season (November–February) in the hyper-arid, arid, and semi-arid zones of Sudan. BMJ, KFT, TDK, and GF are the Betts–Miller–Janjic, improved Kain–Fritch, modified Tiedtke, and Grell–Freitas schemes, respectively. (a) November. (b) December. (c) January. (d) February. (e) November–February

3.4. Discussion

Our modeling experiments revealed that different cumulus parameterization schemes of the WRF model led to different model performance for Sudan. The adjustment type scheme (BMJ) performed better than the mass-flow type schemes (KFT, TDK, and GF) (Figure 3.2a and Figure 3.3a). This result was not consistent with the results of previous studies in the Nile River basin (Tariku and Gan 2018) and the MENA (Zittis et al. 2014a), where the KF outperformed the BMJ. This difference could be attributed to differences in landscapes as well as land cover between these regions. In addition, the fact that the KFT outperformed the BMJ scheme in southeastern Sudan indicates that mass-flux schemes could be used for downscaling over regions of relatively high rainfall in the study area. In the case of the spatial distribution of temperature, the model outputs of both annual and seasonal temperatures were less sensitive to the cumulus parameterization option in the study area (Figure 3.2b,c and Figure 3.3b,c). This conclusion agrees with the results of previous studies of the Nile River basin (Tariku and Gan 2018) and MENA (Zittis et al. 2014a).

Comparisons between climatic zones revealed that the model performance differed between the cumulus parameterization schemes for wet season rainfall (Figure 3.4.). The BMJ outperformed the other schemes for wet season rainfall in the hyper-arid and arid zones. In the semi-arid zone, all four schemes performed relatively poorly for seasonal rainfall, but the mass-flow (KFT) scheme performed better for the main months of the growing season (July and August). This result is consistent with the results of a previous study of cumulus parameterization options for seasonal rainfall in East Africa (Otieno et al. 2020). That study considered the same physics options as this study, and the results showed that mass-flow schemes (KF, KFT, and GD) performed better than the adjustment-type scheme (BMJ). In the case of dry season temperature, the BMJ and TDK schemes outperformed the KFT and GF schemes for TMAX in all three zones (Figure 3.5). In the arid and semi-arid zones, the GF performed better for TMIN during the growing season and its main months (December and January), but the BMJ and TDK outperformed the GF for the seasonal TMIN in the hyper-arid zone (Figure 3.6). This result is partly consistent with the results of a previous study in the Eastern Nile basin, which considered different schemes of the two other physics options (CAM for radiation and MYJ for planetary boundary layer). In that study, the BMJ outperformed the KF and GD schemes (Abdelwares et al. 2018). These results indicate that the model outputs are sensitive to the types of cumulus parameterization options, and the best option

depends on the other physics options considered. Previous studies of WRF downscaling for Northeast Africa (Abdelwares et al. 2018; Tariku and Gan 2018; Otieno et al. 2020) have indicated that the best WRF configuration depends on the type of climate and confirms that the best cumulus parameterization scheme is region-dependent for both rainfall and temperature in the study area. The schemes that performed best for downscaling rainfall during the wet season were the BJM for the hyper-arid and arid zones and the KFT for the semi-arid zone. In the case of dry season temperature, the BMJ and TDK should be used in all climatic zones, but the GF can be selected for TMIN in the arid and semi-arid zones.

3.5. Conclusions

This study evaluated cumulus parameterization options of the WRF model to determine the most robust configuration for a relatively small domain centered over Sudan. The downscaling of the NCEP-CFSR data was sensitive to four schemes, i.e., BMJ, KFT, TDK, and GF. This physics option should be carefully selected for generating high-spatial-resolution climate data in the study area. The major production areas of summer crops lie in the semi-arid zone, whereas irrigated wheat is cultivated mostly in the arid and hyper-arid zones. As rainfall and temperature are determinants of the climatic conditions for summer crops and irrigated wheat, respectively, the recommended schemes for cumulus parameterization are therefore the KFT for wet season rainfall in the semi-arid zone, and either the BMJ or TDK for the dry season temperature in the hyper-arid and arid zones, except for the dry season TMIN in the arid zone, for which the GF is recommended. The cumulus parameterization scheme thus needs to be selected separately for each climatic zone in Sudan.

Chapter 4

Forecasting Yield Anomaly with Statistical Model

4.1. Introduction

An operational system that provides information about crop responses to weather is necessary for early warnings of climate-related crop failure in any country. Crop yield estimates are useful for implementing appropriate agricultural policies (Prasad et al. 2006); in other words, crop yield forecasting in advance of harvest is crucial for the risk management of national food security. For example, yield forecasting helps government decision-makers to relieve food shortages due to weather and climate disasters by organizing international food trade and calling for international aid in advance. Yield forecasting with a long lead time also provides essential information for food trade and commodity markets (Hansen et al. 2004).

Temperature plays an essential role in wheat yield production while precipitation, evapotranspiration, and soil moisture also have an unignorable influence on wheat yield. The warming is slowing yield gains at a majority of wheat-growing areas worldwide and global wheat production is estimated to fall by 6% for each degree of further temperature increase and become more variable over space and time, based on the 30 different crops from Agricultural Model Inter-comparison and Improvement Project (AgMIP) (Asseng et al. 2016). Lobell et al. (2012) found that the increasing of temperature alone, especially the hot extreme, accelerates the senescence of wheat and thus leads to the decrease in the production of wheat in India. A number of the previous studies indicate the increasing of temperature has a strong influence on wheat yield production, especially in the hot and dry environments (Lobell et al. 2008, 2012; Asseng et al. 2016).

While a process-oriented crop growth model has been widely used to estimate the yields of different crops, a simple statistical model is useful for yield forecasting due to the large uncertainty of crop growth model output (Asseng et al. 2015, 2016). In contrast, a simple statistical model can capture the relationship between crop production and climatic driving variables such as temperature (Lobell and Burke 2010). Similar findings were reported from different regions with different statistical models. For instance, simple correlation, multiple linear regression, and other statistical methods are used to analyze wheat yield in Saudi Arabia (Leilah and Al-Khateeb 2005). Multiple regression has been used to identify the significant climate variables for winter wheat

yield prediction in Oklahoma, U.S.A. (Zhang et al. 2017) and employed for wheat yield forecasting in Punjab, India (Bal et al. 2004). Musa et al. (2021) reported that the monthly and seasonal (November–February) temperature indicators, including maximum temperature (TMAX), minimum temperature (TMIN), and frequencies of hot days (maximum temperature above 35 °C) (THD and hot nights (minimum temperature above 20 °C) (THN), show significant relationships with wheat yields in Sudan, and these temperature indicators can be used to develop a multiple regression model for the yield estimates.

While statistical models based on climate-related indicators can be utilized for yield forecasting (Agrawal and Mehta 2007), several models developed for different countries are not satisfactory for their operational use (Bal et al. 2004). One of the reasons is the poor quality of climate data (e.g. coarse spatial resolution). Hence, it is imperative to downscale the climate data (e.g. a 0.5-degree grid) to a higher spatial resolution, and then the downscaled data can be used for yield forecasting as inputs of the statistical models. The WRF model is widely used for this purpose as it provides multiple physics configurations for different regions with different climate backgrounds. For this study region, i.e. Sudan, the best performing configurations have been identified in the previous study (Musa et al. 2022), which provides reliable driving data for yield forecasting.

The main objective of this study was to investigate the feasibility of wheat yield forecasting with a statistical model in Sudan. The specific objectives were (1) to develop a statistical model to estimate the yield anomaly that is solely dependent on temperature, and (2) to evaluate the model performance for the yield estimated using climate forecast data.

4.2. Methods

4.2.1. Datasets

The detrended anomaly of the observed data of the wheat yield in Northern State, Gezira State, and Kassala State for 1970/71–2017/18 and the temperature indicators in Dongola, Wad Medani, and New Halfa for 1970–2018 over the growing season were used for model development. The details of the datasets were described in Musa et al. (2021).

Climate forecast data is generated by using the WRF model, which is driven with seasonal forecast

data from the National Centers for Environmental Prediction-Climate Forecast System Version 2 (CFSv2) Operational Forecasts (https://www.ncei.noaa.gov/access/metadata/landing-page/bin/iso?id=gov.noaa.ncdc:C00877) (Yuan et al. 2011). These data (~ 1° x 1°) for 2011–2018 were downscaled to 10 km horizontal resolution using the WRF model configured with the RRTMG, unified NOAH, YSU, and WSM6 schemes, respectively, corresponding to shortwave and longwave radiation physics, land surface physics, planetary boundary layer physics, and microphysics. The cumulus parameterization scheme varies over different climatic zones and specific temperature index indicators (cf. Chapter 3 and Musa et al. (2022) for the detailed information). With the assumption that the time-series data of the forecasts have the same trend (regression) lines as those of the observations, anomalies of the downscaled data were calculated for model evaluation (cf. Chapter 2 and Musa et al. (2021) for the detrending method).

4.2.2. Model development

A statistical model that estimates the yield (a dependent variable) from the temperature indicators (independent variables) was developed using the backward stepwise regression method. A 10% significance level ($p = 0.1$) was used to eliminate the variables. The regression analysis for each study location (the northern region: Northern State/Dongola, the central region: Gezira State/Wad Medani, and the eastern region: Kassala State/New Halfa) was carried out using the observed data. The independent variables used for the regression analysis were the January, February, and growing-season temperature indicators (TMAX, TMIN, THD, and THN). These two months were included in statistical modeling because of the critical stages of crop growth and development, i.e. heading to flowering in January and ripening in February. The ratio (percentage) data, i.e. THD and THN, were transformed using the logarithm base 10 (log10). The analysis was conducted in SPSS v. 25 software.

4.2.3. Model evaluation

The regression model to be developed was evaluated on a basis of classified yield. The yield anomaly data were classified into three categories: above-normal (the top one-third), near-normal (the middle one-third), and below-normal (the bottom one-third). First, the observed yield was compared with the estimated yield as calculated with the model using the observed temperature data for the 48 crop seasons. Then, the forecasted yield as calculated with the model using the

downscaled temperature data for the seven crop seasons was compared with both the observed and estimated yields for the same period.

The confusion matrix of the three yield classes was used for model evaluation (Table 4.1). The accuracy of the model [the rate of correctly classifying the yield categories] was calculated as (Aa + Nn +Bb) / TOTAL, where TOTAL is the total cases (= Aa + An +Ab +Na +Nn +Nb +Ba + Bn + Bb). The accuracy of the forecasted yield to the observed yield was also calculated to evaluate model performance.

Table 4.1 Confusion matrix of three yield categories (above-normal, near-normal, and below-normal)

		Estimated yield		
		Above-normal (a)	Near-normal (n)	Below-normal (b)
Observed yield	Above-normal (A)	Aa	An	Ab
	Near-normal (N)	Na	Nn	Nb
	Below-normal (B)	Ba	Bn	Bb

4.3. Results and discussion

4.3.1. Northern Region (Northern State/Dongola)

The regression analysis showed that the growing-season THN (THN_{GS}) and February TMAX ($TMAX_{FEB}$) as predictors of the yield (YIELD) have high impacts on yield production in the northern region (Table 4.2). It can be described as the following multiple linear model:

$$Yield = 13.189 - 5306.096 \cdot THN_{GS} - 77.200 \cdot TMAX_{FEB} \quad (1)$$

About 27% of the variance for the yield was explained by the two temperature indicators [R^2 = 0.268, F (2,40) = 7.32, p = 0.02].

Anomalies of the observed yield against the estimated and forecasted yields are shown in Figure 4.1. The accuracy of the estimated yield to the observed yield was 0.50, which was calculated

based on the confusion matrix (Table 4.3). For the period 2012 to 2018, the forecasted anomalies were higher than the observed anomalies (Figure 4.1). The accuracy of the forecasted yield to the observed yield was relatively high (0.43).

The results show that the growing-season THN and February TMAX are the best predictors of the yield prediction model in the northern region of the study area. This agrees with the findings of Musa et al. (2021), which showed that these two temperature indicators were significantly correlated with the yield. The model, which is temperature-dependent, overestimated the yield anomalies for the period 2012 to 2018 (Figure 4.1). This low observed yield, which remarkably decreased after 2007, was due to the change of the government policy on wheat production (Musa et al. 2021). In addition, the predictor TMAX in February, which is the ripening period, should be highlighted because of the critical growth stage. This is supported by the study of Ishag and Mohamed (1996), who emphasized the negative effect of high temperature during grain-filling on wheat grain weight.

Table 4.2 Coefficients of the independent variables (predictors) and their 90% confidence interval (lower and upper bounds) of the regression models for the northern, central, and eastern regions of Sudan (Northern State/Dongola, Gezira State/Wad Medani, and Kassala State/New Halfa, respectively).

Region	Variable	Coefficient	p-value	Lower	Upper
Northern	Constant	13.189	0.865	–116.969	143.346
	THN_{GS}	–5306.096	0.008	–8493.382	–2118.810
	$TMAX_{FEB}$	–77.200	0.033	–136.178	–18.221
Central	Constant	22.053	0.669	–64.151	108.257
	$TMAX_{GS}$	–160.021	0.007	–255.245	–64.797
Eastern	Constant	67.932	0.074	–130.352	–5.512
	$TMIN_{JAN}$	–112.525	0.001	–166.722	–58.328
	THN_{FEB}	–40.260	0.004	–62.551	–17.970

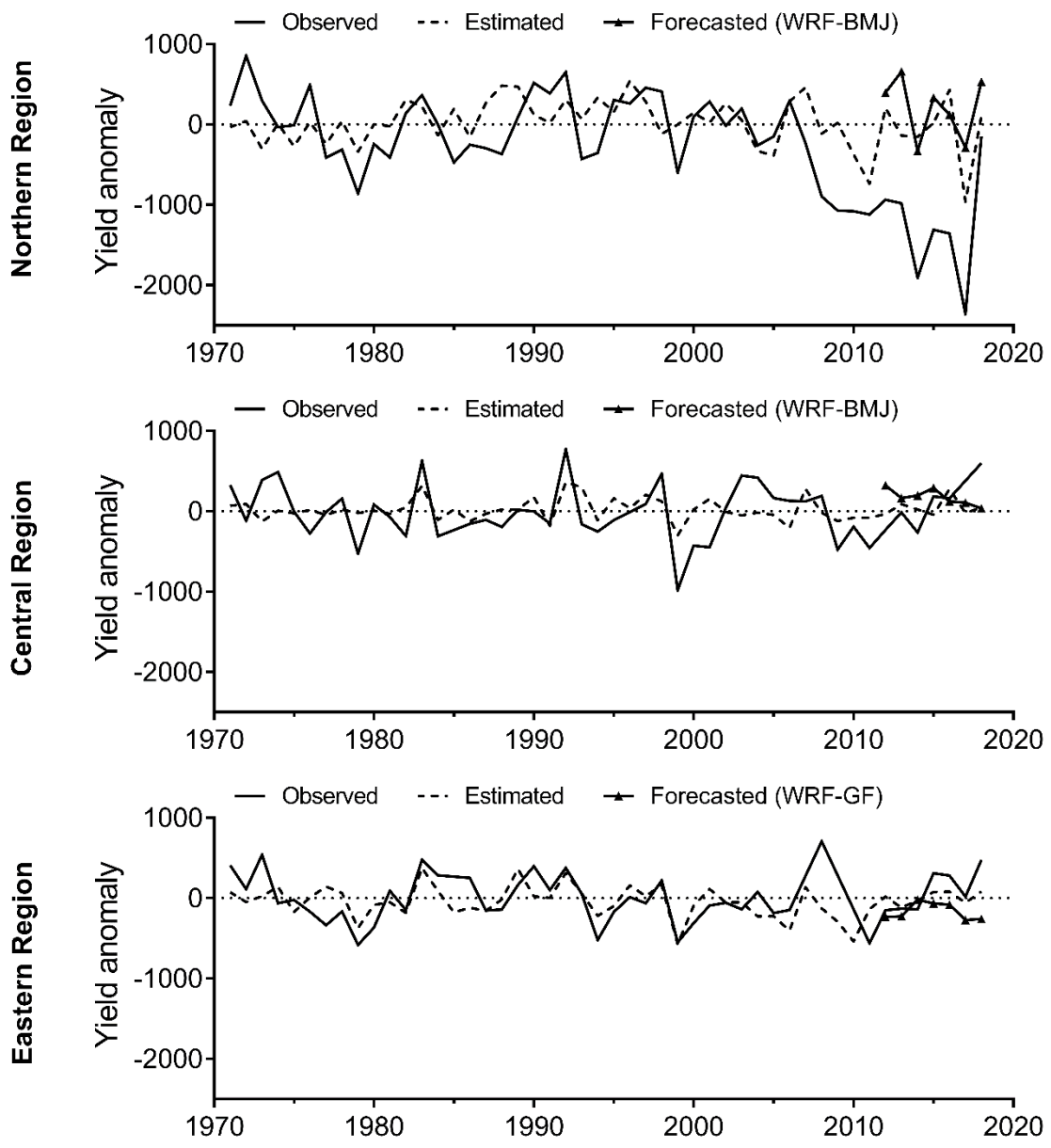

Figure 4.1 Observed, estimated, and forecasted wheat yield from 1971 to 2018 in the northern, central, and eastern regions of Sudan (Northern State/Dongola, Gezira State/Wad Medani, and Kassala State/New Halfa, respectively). WRF-BMJ and WRF-GF were the cumulus parameterization schemes of the WRF model, which were used to downscale the seasonal forecast data (CFSv2).

Table 4.3 Confusion matrices of the observed and estimated yields in the northern, central, and eastern regions of Sudan (Northern State/Dongola, Gezira State/Wad Medani, and Kassala State/New Halfa, respectively).

		Estimated yield		
Northern Region		Above-normal	Near-normal	Below-normal
Observed yield	Above-normal	13	0	3
	Near-normal	10	1	5
	Below-normal	6	0	10
Central Region		Above-normal	Near-normal	Below-normal
Observed yield	Above-normal	3	12	1
	Near-normal	4	10	1
	Below-normal	2	12	1
Eastern Region		Above-normal	Near-normal	Below-normal
Observed yield	Above-normal	7	10	1
	Near-normal	3	11	1
	Below-normal	1	7	7

4.3.2. Central Region (Gezira State/Wad Medani)

A significant regression model for the central region was found with one variable (predictor), i.e. the growing-season TMAX ($TMAX_{GS}$) (Table 4.2), which explains only 17% of the variance for the yield [$R^2 = 0.171$, $F(1,39) = 8.02$, $p = 0.007$]. The estimated yield was less variable than the observed yield, and so does the forecasted (WRF-BMJ) yield (Figure 4.1). The accuracy of the estimated yield to the observed yield was low (0.30) (Table 4.3). The model produced a low variation of the forecasted yield data (Figure 4.1), resulting in the data being classified into a specific yield category, i.e. the near-normal yield.

The growing-season TMAX only identified among the twelve variables is consistent with the result of the correlation analysis in Musa et al. (2021). The low coefficient of determination (R^2) indicates that the yield can be explained by other essential factors such as agronomic management. For instance, Al Zayed et al. (2015) reported that 44% of wheat yield was positively associated with

the total amount of irrigation supply to the cropland in the Gezira Scheme for the period 1970 to 2006. This suggests that irrigation water management is an exoplanetary factor that can be included in the statistical model.

4.3.3 Eastern Region (Kassala State/New Halfa)

The predicters identified for the eastern region were January TMIN ($TMIN_{JAN}$) and February THN (THN_{FEB}) (Table 4.2), explaining about 41% of the variance for the yield [$R^2 = 0.408$, $F(2,38) = 13.12$, $p < 0.001$] with the following multiple linear model:

$$YIELD = 67.932 - 112.525 \cdot TMIN_{JAN} - 40.260 \cdot THN_{FEB} \quad (2)$$

The variation of the observed yield over the period 1971 to 2018 was relatively agreed with that of the estimated yield (Figure 4.1). The accuracy of the estimated yield to the observed yield was 0.52 (Table 4.3). The accuracy of the model for the eastern region was better than that for the central region and equivalent to that for the northern region. The accuracy of the forecasted yield to the observed yield for the eastern region was high (0.86), compared with that for the other two regions.

The predictors of the model to estimate the yield in the eastern region are January TMIN and February THN. This is supported by the study of Musa et al. (2021), which reported that the two predictors were significantly correlated with the yield. The crop is sensitive to minimum temperatures in January and February when the crop is expected to be at the heading, flowering, and ripening stages. This result is supported by Narayanan et al. (2015) and Prasad et al (2008), who reported that high TMIN during flowering and high THN during ripening respectively decrease wheat yield.

4.4. Conclusions

The statistical modeling of the relationship of crop yield with climate variables is useful for developing an operational yield forecast system to reduce risks associated with climate-related hazards. Using the backward stepwise method of multivariate analysis, we developed the statistical models for the yield–temperature relationship in the three wheat-producing areas. The 2-variable

linear regression models were determined for Northern State/Dongola and Kassala State/New Halfa. The variables (predictors) selected by the stepwise regression were the growing-season THN and February TMAX in the northern region, and January TMIN and February THN in the eastern region. The accuracy of the model is moderate; the temperature indicators explain up to about 40% of the variance for the yield. For the central region (Gezira State/Wad Medani), only one predictor (the growing-season TMAX) was selected, hence the low accuracy of the model. Statistical modeling is a potential technique to estimate wheat yield, but additional exoplanetary factors (predictors) such as irrigation water supply will improve the statistical models of irrigated wheat yield prediction in Sudan.

Chapter 5
General Conclusion

5.1. Study findings

As the world's population has increased since the Industrial Revolution, more food is requested to assure food security. In the meantime, climate change leads to its negative effects on crop production in countries vulnerable to increasing climate variability, hence the food crisis. Crop yield outlook is essential for government decision-makers to formulate agricultural policies and climate change adaptation measures. High spatial and temporal resolution data of seasonal weather forecasts are crucial for crop yield prediction. In the study area (Sudan), high temperature during the dry season in wheat-producing areas is a matter of concern. This thesis, therefore, has addressed the statistical analysis of the yield–temperature relationship (Chapter 2), explored the use of the WRF model to generate high resolution climate data (Chapter 3), and conducted statistical modeling for wheat yield estimation from the climate data (Chapter 4).

Similar to global warming in other parts of the world, temperatures are rising in Sudan's wheat production areas, especially in the northern region (Northern State/Dongola) where the minimum temperature (TMIN) is rising rapidly. Wheat yields are negatively affected by the growing-season TMIN and maximum temperature (TMAX). Specifically, they are related to THN (the frequency of hot nights having minimum temperatures above 20 °C) in the northern region, TMAX and THD (the frequency of hot days having maximum temperatures above 35 °C) in the central region (Gezira State/Wad Medani), and TMAX, TMIN, THD, and THN in the eastern region (Kassala State/New Halfa). In addition, temperatures in January, which coincide with the flowering period in the central and eastern regions, have a great impact on the yields. Thus, global warming is progressing in Sudan and will have a negative impact on wheat production in the future.

The optimal configuration of WRF physics options has been identified to generate high spatial resolution data of reanalysis data for specific regional climates in the study area. The model output with the BMJ and TDK schemes produces better downscaled data than that with the other schemes for both TMAX and TMIN during the dry season (wheat growing season) in the hyper-arid zone of Sudan, including the wheat-producing area of the northern region. For the arid zone, including the wheat-producing areas of the central and eastern regions, either the BMJ or TDK scheme can

be used for TMAX, and the GF scheme overperforms for TMIN. In addition, rainfall in the semi-arid region has relatively reproducible with the KFT scheme. Thus, high attention should be paid to selecting the cumulus parameterization scheme for each climatic zone and season in Sudan.

Based on the above-mentioned findings, a stepwise regression model for the yield–temperature relationship has been proposed for each wheat-producing area. The growing-season THN and February TMAX are selected as variables (predictors) of the statistical model for the northern region. For the central region, only one predictor, i.e. the growing-season TMAX, is selected; hence, the low accuracy of the model. For the eastern region, the predictors are January TMIN and February THN, which explain about 40% of the variance for the yield. When model performance is evaluated by classifying the yields into the above-normal, near-normal, and below-normal categories, the accuracy of the forecasted yield to the observed yield is relatively high (86%). Thus, statistical modeling using the stepwise method of multivariate analysis is useful for wheat yield outlook with seasonal forecasts.

The findings of this thesis are summarized as follows: (1) Irrigated wheat yield over the past half-century in the hot environments of Sudan shows an increasing trend and is negatively associated with the growing season temperature; (2) Specific configurations (i.e. cumulus parameterization schemes) of the WRF model are needed for specific seasons and climatic zones; and (3) Temperature-based modeling is a useful method for wheat yield estimation. All in one, the approach for the climate forecast–crop yield modeling based on the historical relationship of wheat yield with temperature can be utilized for developing an early warning system for reducing risks associated with high temperature in the breadbasket of Sudan.

5.2. Future study

While some reliable physics configurations of the WRF model have been identified for the study area, a more extensive model simulation for the sensitivity analysis would be very helpful in a comprehensive configuration for the reliable seasonal forecast. The sensitivity of the WRF model outputs to the choice of physics options has been reported from Northeast Africa. For example, the WSM6 performs better than other microphysics schemes such as GODDARD, WSM3, and WSM5 (Zittis et al. 2014a; Abdelwares et al. 2018), and NOAH performs better than other land surface

schemes such as NOAHMP, CLM, and RUC (Tariku and Gan 2018; Constantinidou et al. 2020). In the case of the planetary boundary layer option, MYJ performs better than YSU over the Nile River basin (Tariku and Gan 2018) and the Eastern Nile basin (Abdelwares et al. 2018), whereas the latter performs better than the former over MENA (Zittis et al. 2014). In the case of the radiation physics option, a set of DUDHIA and RRTM performs better than CAM over the Nile River basin (Tariku and Gan 2018), whereas the latter performs better than the former over the Eastern Nile basin (Abdelwares et al. 2018). The performance of the radiation physics schemes (CAM and RRTMG) for temperature varies from location to location and from season to season over MENA (Zittis and Hadjinicolaou 2017a). In Chapter 3, the other physics options have been fixed to test the cumulus parameterization options. Accordingly, further downscaling experiments for the study area (Sudan) are recommended to evaluate the radiation physics and planetary boundary layer options in particular; for example, RRTMG and YSU can be compared with CAM and MYJ, respectively.

While Chapter 2 has investigated the impact of temperature on wheat yield, it is imperative further to understand the combined effect of climate and agronomic management on irrigated wheat. The government of Sudan has provided large-scale public irrigation schemes (e.g., the Gezira Scheme) with irrigation facilities, fertilizers, pesticides, and improved seeds, but such services are not available for small-scale irrigation schemes scattered along the Nile River in Northern State (Elsheikh et al. 2015). The amount of irrigation water applied to the crop field may be another explanatory factor that can be considered for the yield–temperature relationship in Sudan; for example, the yield of wheat in the Gezira Scheme is correlated with total irrigation water supply from the Sennar Dam (Al Zayed et al. 2015). However, detailed information on irrigation water allocation to wheat is not available; hence, the relationship with the yield remains unknown. Therefore, future study is needed to clarify whether the irrigation information is a key to the yield–temperature relationship analysis. Accordingly, the approach for temperature-based modeling for wheat yield prediction can be improved by incorporating irrigation information in the hot environments of Sudan.

Summary

Sudan is one of the most vulnerable countries to climate variability and change. In particular, agriculture is affected by climate hazards such as drought in the wet season and extremely high temperatures in the dry season. To cope with such hazards, farmers need timely and reliable climate information for agronomic management, including seed planting, fertilizer application, and irrigation scheduling. Crop yield prediction can help in coping with climate-related risks of yield reduction by taking mitigation measures. For that, the interpretation of seasonal climate forecasts is important as a way to predict crop yield before the growing season. Further, crop yield estimation is required for the process of decision-making in food policy on a regional scale. For example, the outlook for cereal production prior to harvest is crucial for the government decision-makers to plan grain imports beforehand in case of shortages. Thus, early warning systems for climate risk management in crop production have gained worldwide attention. However, the current spatial resolution of the climate forecast data is not high enough for operational use in estimating crop yield, and also high spatial resolution climate data are required for local-scale impact assessments of climate variability. The outputs of general circulation models (GCMs) are not sufficient for such local-scale studies, and therefore regional climate models (RCMs), which incorporate detailed specifications of the earth's surface such as land use and water bodies, have been broadly applied to satisfy this requirement. Weather Research and Forecasting (WRF) is a well-known RCM used for many purposes such as operational forecasting and dynamical downscaling. As local climates are regulated by global atmospheric circulations with RCM's initial and boundary conditions and further constrained by land surface conditions, the WRF model can be configured with multiple physics options such as cumulus parameterization schemes to satisfy region-dependent climate conditions.

Wheat is one of the most important grains in the world and contributes significantly to food security in many countries. The demand for wheat production is increasing due to the increase of the world's population, and so does Sudan. In Sudan, wheat is cultivated under irrigation during the hot and dry season, but high temperature has a negative impact on the crop growth. While improving the heat tolerance of cultivars is one of the reliable measures to adapt to climate change, a yield outlook system with high spatial resolution data of seasonal forecasts is a valuable tool to cope with climate variability. The aim of this thesis was therefore to develop an approach for crop yield prediction with regard to the impact of high temperature on wheat production. The main objectives were (1) to investigate the regional-scale relationship of wheat yields with temperature for the last five decades, (2) to identify a robust configuration of the WRF model for generating high-spatial-resolution climate data for crop growing seasons, and (3) to study the feasibility of wheat yield forecasting.

First, the association between yield of irrigated wheat in hot drylands of Sudan and temperature during the growing season (November–February) was determined. Regional-scale yield data in

three major wheat-producing areas (Northern State, Gezira State, and Kassala State) in 48 crop seasons (1970/71–2017/18) were used to determine the correlation of yield with maximum (TMAX) and minimum temperatures (TMIN) at representative meteorological stations (Dongola, Wad Medani, and New Halfa, respectively). Frequencies of days with maximum temperature above 35 °C (THD) and minimum temperature above 20 °C (THN) were also used for correlation analysis. In all three areas, regression analysis detected upward trends in the growing-season temperature. The increase in temperature was particularly evident at Dongola, although no such trend has been reported previously. The yields were negatively correlated with the growing-season temperature, particularly THN in Northern State, TMAX in Gezira State, and TMIN in Kassala State. These results confirm that the recent increase in the growing-season temperature might have reduced the yield to some extent in the breadbasket of Sudan.

Second, robust configurations of the WRF model, especially cumulus parameterization schemes, for different climatic zones of Sudan were identified, focusing on wet season (June–September) rainfall and dry season (November–February) temperature, which are determinants of summer crop and irrigated wheat yields, respectively. Downscaling experiments were carried out to compare the following schemes: Betts–Miller–Janjic (BMJ), improved Kain–Fritch (KFT), modified Tiedtke (TDK), and Grell–Freitas (GF). Results revealed that the BMJ performed better for wet season rainfall in the hyper-arid and arid zones; KFT performed better for rainfall in July and August in the semi-arid zone where most summer crops are cultivated. For dry season temperature, the BMJ and TDK outperformed the other two schemes in all three zones, except that the GF performed best for the minimum temperature in December and January in the arid zone (Gezira State/Wad Medani and Kassala State/New Halfa), where irrigated wheat is produced, and in the semi-arid zone. Specific cumulus parameterization schemes of the WRF model therefore need to be selected for specific seasons and climatic zones of Sudan.

Third, statistical models for the yield–temperature relationship in the three wheat-producing areas were developed using the backward stepwise regression method. The 2-variable linear regression models were determined for the northern and eastern regions (Northern State/Dongola and Kassala State/New Halfa, respectively). The variables (predictors) selected by the stepwise regression were the growing-season THN and February TMAX in the northern region, and January TMIN and February THN in the eastern region, explaining up to about 40% of the variance for the yield. For the central region (Gezira State/Wad Medani), only one predictor (the growing-season TMAX) was selected, hence the low accuracy of the model. For the eastern region, when model performance was evaluated by classifying the yields into the above-normal, near-normal, and below-normal categories, the accuracy of the forecasted yield to the observed yield was relatively high (86%). Thus, statistical modeling using the stepwise method of multivariate analysis is a useful method for wheat yield outlook with seasonal forecasts.

The findings of this thesis are summarized as follows: (1) Irrigated wheat yield over the past half-century in the hot environments of Sudan shows an increasing trend and is negatively associated with the growing season temperature; (2) Specific configurations (i.e. physics options) of the WRF model in spatial downscaling of climate data are needed for specific seasons and climatic zones; and (3) Temperature-based statistical modeling is a useful method for wheat yield estimation in the irrigation areas of Sudan. Based on these findings, it was concluded that the yield outlook prior to the growing season is possible by incorporating high spatial resolution climate forecasts into the statistical model for yield estimation. Accordingly, the approach developed in this thesis contributes to developing an early warning system for reducing risks associated with high temperature in the wheat production areas of Sudan.

Summary in Japanese

スーダンは、気候変化および気候変動に脆弱な国の一つである。特に、スーダン国内の農業は雨季の干ばつや乾季の極端な高温などの気候ハザードに大きく影響を受ける。このようなハザードに対処するために、農家は、播種、施肥、灌漑計画など、栽培管理のためのタイムリーで信頼性の高い気候情報を必要としている。気候関連の収量減少リスクへの緩和策を講じるには、収量予測が有用であり、生育期前に収量を予測する方法として季節予報の解釈が重要である。さらに、作物収量の推定は、地域規模での食糧政策の意思決定プロセスにおいて重要な役割を担っている。たとえば、政府の意思決定者が食糧不足に備えて穀物の輸入を計画するためには、収穫期前に穀物生産量の見通しを立てておくことが必要となる。このような理由から、作物生産における気候リスク管理のための早期警報システムは世界的に注目を集めている。ただし、現在の気候予測データの空間解像度は、作物収量の推定に活用するには十分でなく、また気候変動影響を地域規模で評価するには、高空間解像度の気候データが必要である。大気大循環モデル（GCMs）の出力は、このような地域規模研究への適用には不十分であるため、土地利用や水域などの地表の詳細な仕様を組み込み、不足を補うことができる領域気候モデル（RCMs）が広く適用されている。Weather Research and Forecasting（WRF）は、運用予測や動的ダウンスケーリングなどの多くの目的で使用される広く知られた RCM である。局地気候は RCM の初期条件および境界条件が地球規模の大気循環によって制御され、地表条件により更に制約されるため、WRF モデルは、地域に依存する気候条件を満たす積雲パラメータ化スキームといった複数の物理過程オプションを設定することができる。

多くの国において食料安全保障に大きく影響するコムギは、世界で最も重要な穀物の一つであるが、世界人口の増加により、スーダンを含む世界各国で生産の需要が高まっている。スーダンにおいてコムギは、高温で乾燥した時期に灌漑で栽培されているが、高温はコムギの生育に負の影響を及ぼす。品種の耐暑性を向上することは、気候変化への適応において有効であるが、高空間解像度の気候予測を用いた収量見通しシステムは、増大する気候変動への対処に有効である。したがって、本研究は、コムギ生産における高温の影響を反映した作物収量予測の手法を開発することを目的とした。具体的には、（1）地域規模における過去 50 年間のコムギ収量と気温の関係を調査し、（2）作物生育期の高空間解像度の気候データを生成するための堅牢な WRF モデルの構成を特定し、（3）コムギ収量予測の実現可能性を検討した。

第一に、スーダンの高温乾燥地における灌漑栽培コムギの収量と生育期にあたる 11 月から 2 月の気温との関係を明らかにした。スーダンの主要なコムギ生産地である北部州、ゲジラ州、およびカッサラ州の 3 地域において、1970/71 年から 2017/18 年の 48 年間の地域規模収量データを用いて、主要な気象観測地点であるドンゴラ、ワドメダニ、ニューハルファそれぞれの収量と最高気温（TMAX）および最低気温（TMIN）の相関分析を行った。この際、最高気温が 35℃以上となった日の発生頻度（THD）および最低気温が 20℃以上となった日の発生頻度（THN）も考慮した。回帰分析の結果、３つの全ての地域で、生育期の気温の上昇傾向が検出された。気温の上昇はドンゴラにおいて特に顕著であったが、過去にそのような傾向は報告されてない。収量は生育期の気温と負の相関を示し、特に北部州の THN、ゲジラ州の TMAX およびカッサラの TMIN と

の相関が顕著であった。これらの結果から、スーダンの穀倉地帯のコムギ収量の低下は、近年の生育期における気温上昇に起因する可能性があるということが示唆された。

第二に、スーダンの異なる気候帯における、夏作物の収量の決定要因である雨期（6月～9月）の降雨量および、灌漑栽培コムギの収量決定要因である乾季（11月～2月）の気温について、WRFモデルにおいて最適な積雲パラメータ化スキームを選定した。ダウンスケール実験では、Betts–Miller–Janjic（BMJ）、改良型Kain–Fritch（KFT）、修正型Tiedtke（TDK）、およびGrell–Freitas（GF）の各スキームを比較した。その結果、極乾燥地帯および乾燥地帯の雨季の降雨に対してBMJがより良いパフォーマンスを示し、 KFTは夏作物のほとんどが栽培される半乾燥地帯の7月と8月の降雨量に対してより良いパフォーマンスを示した。乾季の気温については、BMJとTDKは3つの地域すべてで他の2つのスキームより良いパフォーマンスを示した。しかし、半乾燥地帯および、ゲジラ州ワドメダニやカッサラ州ニューハルファの灌漑栽培コムギが生産される乾燥地帯における12月および1月の最低気温のダウンスケールではGFが最高のパフォーマンスを示した。したがって、スーダンの特定の季節と気候帯に対しては、特定の積雲パラメータ化スキームを選択する必要があるといえる。

第三に、3つのコムギ生産地域における収量と気温の関係について、後退型ステップワイズ回帰法を用いて統計モデルを開発した。北部州ドンゴラを含む北部地域およびカッサラ州ニューハルファを含む東部地域については、2変数線形回帰モデルが選択された。ステップワイズ回帰により、北部地域では生育期のTHNと2月のTMAX、東部地域では1月のTMINと2月のTHNが変数（予測子）として選択された。この変数は収

量分散の最大約 40%を説明することができた。ゲジラ州ワドメダニを含む中央地域では、唯一生育期の TMAX が予測子として選択されたため、モデルの精度が低かった。東部地域では、モデルのパフォーマンスを、平年以上、平年並み、平年以下の収量カテゴリに分類して評価した場合、実際の収量に対する予測収量の精度は 86%と比較的高かった。したがって、多変量解析のステップワイズ法を用いた統計モデリングは、季節予報によるコムギの収量見通しに有用であるといえる。

本研究では、（1）スーダンの高温環境において、過去半世紀にわたり灌漑栽培コムギの収量が増加傾向を示し、生育期の気温と負の関係にあること、（2）気候データの空間的ダウンスケーリングにおいて、特定の季節および気候帯により、WRF モデルに特定の物理過程オプションを選択する必要があること、（3）スーダンの灌漑地におけるコムギの収量推定において、気温ベースの統計モデリング手法が有用であることが明らかになった。これらの結果から、高空間解像度の気候予測を収量推定の統計モデルに組み込むことにより、生育期前の収量見通しが可能であると結論付けられた。したがって、本研究で開発された手法は、スーダンのコムギ生産地における高温に伴うリスクを軽減するための早期警戒システムの開発に寄与する。

References

Abdelwares M, Haggag M, Wagdy A, Lelieveld J (2018) Customized framework of the WRF model for regional climate simulation over the Eastern NILE basin. Theor Appl Climatol 2018 134:1135–1151

Adam HS, Ageeb OOA (1994) Temperature analysis and wheat yields in the Gezira scheme. In Saunders DA, Hettel GP (eds) Wheat in heat-stressed environments: irrigated, dry areas and rice-wheat farming systems. CIMMYT, Mexico DF, pp 143–145

Adeniyi MO (2019) Sensitivities of the Tiedtke and Kain-Fritsch convection schemes for RegCM4.5 over West Africa. Meteorol Hydrol Water Manag 7: 27–37

Agrawal R, Mehta SC (2007) Weather based forecasting of crop yields, pests and diseases-IASRI models. J Ind Soc Agril Stat 61:255–263

Al Zayed IS, Elagib NA, Ribbe L, Heinrich J (2015) Spatio-temporal performance of large-scale Gezira Irrigation Scheme, Sudan. Agric Syst 133:131–142

Al-Feel MA, Al-Basheer AAR (2012) Economic efficiency of wheat production in Gezira scheme, Sudan. J Saudi Soc Agric Sci 11:1–5

Asfaw D, Black E, Brown M, Nicklin KJ, Otu-Larbi F, Pinnington E, Challinor A, Maidment R, Quaife T (2018) TAMSAT-ALERT v1: a new framework for agricultural decision support. Geosci Model Dev 11:2353–2371.

Asseng S, Foster IAN, Turner NC (2011) The impact of temperature variability on wheat yields. Glob Chang Biol 17:997–1012

Asseng S, Ewert F, Martre P, Rötter RP, Lobell DB, Cammarano D, Kimball BA, Ottman MJ, Wall GW, White JW, Reynolds MP, Alderman PD, Prasad PVV, Aggarwal PK, Anothai J, Basso B, Biernath C, Challinor AJ, De Sanctis G, Doltra J, Fereres E, Garcia-Vila M, Gayler S, Hoogenboom G, Hunt LA, Izaurralde RC, Jabloun M, Jones CD, Kersebaum KC, Koehler A-K, Müller C, Naresh Kumar S, Nendel C, O'Leary G, Olesen JE, Palosuo T, Priesack E, Eyshi Rezaei E, Ruane AC, Semenov MA, Shcherbak I, Stöckle C, Stratonovitch P, Streck T, Supit I, Tao F, Thorburn PJ, Waha K, Wang E, Wallach D, Wolf J, Zhao Z, Zhu Y (2015) Rising temperatures reduce global wheat production. Nat Clim Chang 5:143

Asseng S, Cammarano D, Basso B, et al (2017) Hot spots of wheat yield decline with rising temperatures. Glob Chang Biol 23:2464–2472

Bal SK, Mukherjee J, Mallick K, Hundal SS (2004) Wheat yield forecasting models for Ludhiana district of Punjab state. J Agrometeorol 6:161–165

Betts AK, Miller MJ (1986) A new convective adjustment scheme. Part II: Single column tests using GATE wave, BOMEX, ATEX and arctic air-mass data sets. Q J R Meteorol Soc 112:693–709

Bonan GB (1996) A land surface model (LSM version 1.0) for ecological, hydrological, and atmospheric studies: technical description and user's guide, NCAR Technical Note NCAR/TN-417+STR; National Center for Atmospheric Research: Boulder, CO, USA, 150p

Brisson N, Gate P, Gouache D, Charmet G, Oury F-X, Huard F (2010) Why are wheat yields stagnating in Europe? A comprehensive data analysis for France. Field Crops Res 119:201–212

Calzadilla A, Rehdanz K, Betts R, et al (2013) Climate change impacts on global agriculture. Clim Change 120:357–374

Christensen JH, Carter TR, Rummukainen M (2007) Evaluating the performance and utility of regional climate models: the PRUDENCE project. Clim Change 81:1–6

Collins DA, Della-Marta PM, Plummer N, Trewin BC (2000) Trends in annual frequencies of extreme temperature events in Australia. Aust Meteorol Mag 49:277–292

Collins WD, Rasch PJ, Boville BA, Hack JJ, McCaa JR, Williamson DL, Briegleb BP, Bitz CM, Lin SJ, Zhang M (2006) The formulation and atmospheric simulation of the Community Atmosphere Model Version 3 (CAM3). J Clim 19:2144–2161

Constantinidou K, Hadjinicolaou P, Zittis G, Lelieveld J (2020) Performance of land surface schemes in the WRF model for climate simulations over the MENA-CORDEX domain. Earth Syst Environ 4:647–665

Dudhia J (1989) Numerical study of convection observed during the winter monsoon experiment using a mesoscale two–dimensional model. J Atmos Sci 46:3077–3107

Dudhia J (2014) A history of mesoscale model development. Asia-Pacific J Atmos Sci 50:121–131

Elagib NA (2010) Trends in intra-and inter-annual temperature variabilities across Sudan. Ambio 39:413–429

Elagib NA (2013) Meteorological drought and crop yield in sub-Saharan Sudan. Int J Water Resour Arid Environ 2: 164–171

Elagib NA, Mansell MG (2000) Recent trends and anomalies in mean seasonal and annual temperatures over Sudan. J Arid Environ 45:263–288

Elsheikh OE, Elbushra AA, Salih AAA (2015) Economic impacts of changes in wheat's import tariff on Sudanese economy. J Saudi Soc Agric Sci 14:68–75

FAO (2012) Harmonized World Soil Database (version 1.2). Food Agriculture Organization, Rome, Italy and IIASA, Laxenburg, Austria

FAO (2019) FAO Crop and Food Supply Assessment Mission to the Sudan – Special Report. Rome

Faki HHM, Ismail MA (1994) Some indicators for wheat production prospects in Sudan. In: Saunders DA, Hettel GP (eds), Wheat in heat-stressed environments: irrigated, dry areas and rice-wheat farming systems. CIMMYT, Mexico DF, pp 96–104

Fritsch JM, Chappell CF (1980) Numerical prediction of convectively driven mesoscale pressure systems. Part I: Convective parameterization. J Atmos Sci 37:1722–1733

Fu C, Wang S, Xiong Z, Gutowski WJ, Lee DK, McGregor JL, Sato Y, Kato H, Kim JW, Suh MS (2005) Regional Climate Model Intercomparison Project for Asia. Bull Amer Meteor Soc 86:257–266

Garcia-Carreras L, Challinor AJ, Parkes BJ, Birch CE, Nicklin KJ, Parker DJ (2015) The impact of parameterized convection on the simulation of crop processes. J Appl Meteorol Climatol 54:1283–1296

García GA, Dreccer MF, Miralles DJ, Serrago RA (2015) High night temperatures during grain number determination reduce wheat and barley grain yield: a field study. Glob Chang Biol 21:4153–4164

García GA, Serrago RA, Dreccer MF, Miralles DJ (2016) Post-anthesis warm nights reduce grain weight in field-grown wheat and barley. Field Crops Res 195:50–59

Gebrechorkos SH, Hülsmann S, Bernhofer C (2019) Changes in temperature and precipitation extremes in Ethiopia, Kenya, and Tanzania. Int J Climatol 39:18–30

Gelaro R, McCarty W, Suárez MJ, Todling R, Molod A, Takacs L, Randles CA, Darmenov A, Bosilovich MG, Reichle R, Wargan K, Coy L, Cullather R, Draper C, Akella S, Buchard V, Conaty A, da Silva AM, Gu W, Kim GK, Koster R, Lucchesi R, Merkova D, Nielsen JE, Partyka G, Pawson S, Putman W, Rienecker M, Schubert SD, Sienkiewicz M, Zhao B (2017)

The Modern-Era Retrospective Analysis for Research and Applications, Version 2 (MERRA-2). J Clim 30:5419–5454

Gil-Alana LA, Yaya OS, Fagbamigbe AF (2019) Time series analysis of quarterly rainfall and temperature (1900–2012) in sub–Saharan African countries. Theor Appl Climatol 137:61–76

Giorgi F, Jones C, Asrar GR (2009) Addressing climate information needs at the regional level: the CORDEX framework. WMO Bull 58:175–183

Grell GA (1993) Prognostic evaluation of assumptions used by cumulus parameterizations. Mon Weather Rev 121:764–787

Grell GA, Dévényi D (2002) A generalized approach to parameterizing convection combining ensemble and data assimilation techniques. Geophys Res Lett 29:31–38

Grell GA, Freitas SR (2014) A scale and aerosol aware stochastic convective parameterization for weather and air quality modeling. Atmos Chem Phys 14:5233–5250

Hansen JW, Potgieter A, Tippett MK (2004) Using a general circulation model to forecast regional wheat yields in northeast Australia. Agric For Meteorol 127:77–92

Hatfield JL, Boote KJ, Kimball BA, Ziska LH, Izaurralde RC, Ort D, Thomson AM, Wolfe DW (2011) Climate impacts on agriculture: implications for crop production. Agron J 103:351–370

Hatfield JL, Prueger JH (2015) Temperature extremes: Effect on plant growth and development. Weather Clim Extrem 10:4–10

Hlavinka P, Trnka M, Semerádová D, Dubrovský M, Žalud Z, Možný M (2009) Effect of drought on yield variability of key crops in Czech Republic. Agric For Meteorol 149:431–442

Hong SY, Dudhia J, Chen SH (2004) A revised approach to ice microphysical processes for the bulk parameterization of clouds and precipitation. Mon Weather Rev 132:103–120

Hong SY, Lim JOJ (2006) The WRF single-moment 6-class microphysics scheme (WSM6). Asia-Pacific J Atmos Sci 42:129–151

Hong SY, Noh Y, Dudhia J (2006) A new vertical diffusion package with an explicit treatment of entrainment processes. Mon Weather Rev 134:2318–2341

Huang J, Yu H, Guan X, Wang G, Guo R (2016) Accelerated dryland expansion under climate change. Nat Clim Change 6, 166–171

Huang J, Yu H, Dai A, Wei Y, Kang L (2017) Drylands face potential threat under 2 °C global warming target. Nat Clim Change 7, 417–422

Huffman GJ, Bolvin DT, Braithwaite D, Hsu KL, Joyce RJ, Kidd C, Nelkin EJ, Sorooshian S, Stocker EF, Tan J, Wolff DB, Xie P (2020) Integrated multi-satellite retrievals for the Global Precipitation Measurement (GPM) mission (IMERG). In Satellite Precipitation Measurement, Advances in Global Change Research, Vol. 67; Levizzani V, Kidd C, Kirschbaum DB, Kummerow CD. Nakamura K. Turk FJ. Eds, Springer, Cham, pp 343–353

IPCC (2014) Climate Change 2014: Impacts, Adaptation, and Vulnerability. Part A: Global and Sectoral Aspects. Contribution of Working Group II to the Fifth Assessment Report of the Intergovernmental Panel on Climate Change [Field CB, Barros VR, Dokken DJ, Mach KJ, Mastrandrea MD, Bilir TE, Chatterjee M, Ebi KL, Estrada YO, Genova RC, Girma B, Kissel ES, Levy AN, MacCracken S, Mastrandrea PR, White LL (eds.)]. Cambridge University Press, Cambridge, United Kingdom and New York, NY, USA

IPCC (2019) Climate Change and Land: an IPCC special report on climate change, desertification, land degradation, sustainable land management, food security, and greenhouse gas fluxes in terrestrial ecosystems [Shukla PR, Skea J, Calvo Buendia E, Masson-Delmotte V, Pörtner H-O, Roberts DC, Zhai P, Slade R, Connors S, van Diemen R, Ferrat M, Haughey E, Luz S, Neogi S, Pathak M, Petzold J, Portugal Pereira J, Vyas P, Huntley E, Kissick K, Belkacemi M, Malley J (eds.)]

Iacono MJ, Delamere JS, Mlawer EJ, Shephard MW, Clough SA, Collins WD (2008) Radiative forcing by long-lived greenhouse gases: Calculations with the AER radiative transfer models. J Geophys Res 113:D13103

Igri PM, Tanessong RS, Vondou DA, Panda J, Garba A, Mkankam FK, Kamga A (2018) Assessing the performance of WRF model in predicting high-impact weather conditions over Central and Western Africa: an ensemble-based approach. Nat Hazards 93:1565–1587

Iizumi T, Shiogama H, Imada Y, Hanasaki N, Takikawa H, Nishimori M (2018) Crop production losses associated with anthropogenic climate change for 1981–2010 compared with preindustrial levels. Int J Climatol 38:5405–5417

Iizumi T, Ali-Babiker IEA, Tsubo M, Tahir ISA, Kurosaki Y, Kim W, Gorafi YSA, Idris AAM, Tsujimoto H (2021) Rising temperatures and increasing demand challenge wheat supply in Sudan. Nat Food 2:19–27.

Ishag HM, Mohamed BA (1996) Phasic development of spring wheat and stability of yield and its components in hot environments. Field Crops Res 46:169–176

Janjić ZI (1994) The step-mountain eta coordinate model: Further developments of the convection, viscous sublayer, and turbulence closure schemes. Mon Weather Rev 122:927–945

Kain JS (2004) The Kain-Fritsch convective parameterization: an update. J Appl Meteorol 43:170–181

Kain JS, Fritsch JM (1993) Convective parameterization for mesoscale models: The Kain-Fritcsh scheme. In The Representation of Cumulus Convection in Numerical Models, Emanuel KA, Raymond DJ, Eds., American Meteorological Society, Boston, MA, USA, 246p

Leilah AA, Al-Khateeb SA (2005) Statistical analysis of wheat yield under drought conditions. J Arid Environ 61:483–496

Licker R, Kucharik CJ, Doré T, Lindeman MJ, Makowski D (2013) Climatic impacts on winter wheat yields in Picardy, France and Rostov, Russia: 1973–2010. Agric For Meteorol 176:25–37

Lobell DB, Field CB (2007) Global scale climate–crop yield relationships and the impacts of recent warming. Environ Res Lett 2:014002

Lobell DB, Ortiz-Monasterio JI, Asner GP, Matson PA, Naylor RL, Falcon WP (2005) Analysis of wheat yield and climatic trends in Mexico. Field Crops Res 94:250–256

Lobell DB, Schlenker W, Costa-Roberts J (2011) Climate Trends and Global Crop Production Since 1980. Science 333:616–620

Lobell DB, Bonfils CJ, Kueppers LM, Snyder MA (2008) Irrigation cooling effect on temperature and heat index extremes. Geophys Res Lett 35:

Lobell DB, Burke MB (2010) On the use of statistical models to predict crop yield responses to climate change. Agric For Meteorol 150:1443–1452

Lobell DB, Sibley A, Ivan Ortiz-Monasterio J (2012) Extreme heat effects on wheat senescence in India. Nat Clim Chang 2:186–189

Ma LM, Tan ZM (2009) Improving the behavior of the cumulus parameterization for tropical cyclone prediction: convection trigger. Atmos Res 92:190–211

Mearns LO, Sain S, Leung LR, Bukovsky MS, McGinnis S, Biner S, Caya D, Arritt RW, Gutowski W, Takle E, Snyder M, Jones RG, Nunes AMB, Tucker S, Herzmann D, McDaniel L, Sloan L (2013) Climate change projections of the North American Regional Climate Change Assessment Program (NARCCAP). Clim Change 120:965–975

Mengistu D, Bewket W, Lal R (2014) Recent spatiotemporal temperature and rainfall variability and trends over the Upper Blue Nile River Basin, Ethiopia. Int J Climatol 34:2278–2292

Middleton N, Thomas DSG (1992) World atlas of desertification. UNDP/Edward Arnold: London, UK, 69p

Mitchell K, Ek M, Wong V, Lohmann D, Koren V, Schaake J, Duan Q, Gayno G, Moore B, Grunmann P, Tarpley D, Ramsay B, Chen F, Kim J, Pan HL, Lin Y, Marshall C, Mahrt L, Meyers T, Ruscher P (2005) Noah land surface model (LSM) user's guide. NCAR Research Application Laboratory, Bolder, CO, USA, 26p

Mlawer EJ, Taubman SJ, Brown PD, Iacono MJ, Clough SA (1997) Radiative transfer for inhomogeneous atmospheres: RRTM, a validated correlated-k model for the longwave. J Geophys Res:Atmos 102(D14):16663–16682

Moore FC, Lobell DB (2015) Climate fingerprint on European crop yields. Proc Natl Acad Sci USA 112:2670–2675

Morgounov A, Sonder K, Abugalieva A, Bhadauria V, Cuthbert RD, Shamanin V, Zelenskiy Y, DePauw RM (2018) Effect of climate change on spring wheat yields in North America and Eurasia in 1981–2015 and implications for breeding. PLoS One 13:e0204932

Mugume I, Waiswa D, Mesquita MDS, Reuder J, Basalirwa C, Bamutaze Y, Twinomuhangi R, Tumwine F, Sansa Otim J, Jacob Ngailo T, Ayesiga G (2017) Assessing the performance of WRF model in simulating rainfall over western Uganda. J Climatol Weather Forecast 5:1000197

Musa AII, Tsubo M, Ali-Babiker IA, Iizumi T, Kurosaki Y, Ibaraki Y, El-Hag FMA, Tahir ISA, Tsujimoto H (2021) Relationship of irrigated wheat yield with temperature in hot environments of Sudan. Theor Appl Climatol 145: 1113–1125

Musa AII, Tsubo M, Ma S, Kurosaki Y, Ibaraki Y, Ali-Babiker I A (2022) Evaluation of WRF Cumulus Parameterization Schemes for the Hot Climate of Sudan Emphasizing Crop Growing Seasons. Atmosphere 13:572

NOAA National Centers for Environmental Information (2020) State of the Climate: Global Climate Report – Annual 2019. https://www.ncdc.noaa.gov/sotc/global/201913. Accessed 14 September 2020

Narayanan S, Prasad PV V, Fritz AK, Boyle DL, Gill BS (2015) Impact of high night-time and high daytime temperature stress on winter wheat. J Agron Crop Sci 201:206–218

Negassa A, Shiferaw B, Koo J, et al (2013) The potential for wheat production in Africa: analysis of biophysical suitability and economic profitability. CIMMYT, Mexico, DF

Nicholls N (1997) Increased Australian wheat yield due to recent climate trends. Nature 387:484–485

Niu GY, Yang ZL, Mitchell KE, Chen F, Ek MB, Barlage M, Kumar A, Manning K, Niyogi D, Rosero E, Tewari M, Xia Y (2011) The community Noah land surface model with multiparameterization options (Noah-MP): 1. Model description and evaluation with local-scale measurements. J Geophys Res Atmos 116:D12109

Nsubuga FW, Olwoch JM, Rautenbach H (2014) Variability properties of daily and monthly observed near-surface temperatures in Uganda: 1960–2008. Int J Climatol 34:303–314

Nuttall JG, Barlow KM, Delahunty AJ, Christy BP, O'Leary GJ (2018) Acute high temperature response in wheat. Agron J 110:1296–1308

Omondi PA, Awange JL, Forootan E, Ogallo LA, Barakiza R, Girmaw GB, Fesseha I, Kululetera V, Kilembe C, Mbati MM, Kilavi M, King'uyu SM, Omeny PA, Njogu A, Badr EM, Musa TA, Muchiri P, Bamanya D, Komutunga E (2014) Changes in temperature and precipitation extremes over the Greater Horn of Africa region from 1961 to 2010. Int J Climatol 34:1262–1277

Ongoma V, Chen H (2017) Temporal and spatial variability of temperature and precipitation over East Africa from 1951 to 2010. Meteorol Atmos Phys 129:131–144

Otieno G, Mutemi JN, Opijah FJ, Ogallo LA, Omondi MH (2020) The sensitivity of rainfall characteristics to cumulus parameterization schemes from a WRF model. Part I: A case study over East Africa during wet years. Pure Appl Geophys 177:1095–1110

Porter JR, Gawith M (1999) Temperatures and the growth and development of wheat: a review. Eur J Agron 10:23–36

Prasad AK, Chai L, Singh RP, Kafatos M (2006) Crop yield estimation model for Iowa using remote sensing and surface parameters. Int J Appl earth Obs Geoinf 8:26–33

Prasad PVV, Pisipati SR, Ristic Z, Bukovnik U, Fritz AK (2008) Impact of nighttime temperature on physiology and growth of spring wheat. Crop Sci 48:2372–2380

Ratna SB, Ratnam JV, Behera SK, Rautenbach CJdeW, Ndarana T, Takahashi K, Yamagata T (2014) Performance assessment of three convective parameterization schemes in WRF for downscaling summer rainfall over South Africa. Clim Dyn 42:2931–2953

Ray DK, West PC, Clark M, Gerber JS, Prishchepov AV, Chatterjee S (2019) Climate change has likely already affected global food production. PLoS One 14(5):e0217148

Saha S, Moorthi S, Pan HL, Wu X, Wang J, Nadiga S, Tripp P, Kistler R, Woollen J, Behringer D, Liu H, Stokes D, Grumbine R, Gayno G, Wang J, Hou YY, Chuang Y, Juang HMH, Sela J, Iredell M, Treadon R, Kleist D, Van Delst P, Keyser D, Derber L, Ek M, Meng J, Wei H, Yang R, Lord S, van den Dool H, Kumar A, Wang W, Long C, Chelliah M, Xue Y, Huang B, Schemm JK, Ebisuzaki W, Lin R, Xie P, Chen M, Zhou S, Higgins W, Zou CZ, Liu Q, Chen Y, Han Y, Cucurull L, Reynolds RW, Rutledge G, Goldberg M (2010) The NCEP climate forecast system reanalysis. Bull Am Meteorol Soc 91:1015–1058

Skamarock WC, Klemp JB, Dudhia J, Gill DO, Liu Z, Berner J, Wang W, Powers JG, Duda MG, Barker DM, Huang, XY (2019) A Description of the Advanced Research WRF Model Version 4.1. NCAR Technical Notes NCAR/TN-556+STR. National Center for Atmospheric Research: Boulder, CO, USA, 145p

Smirnova TG, Brown JM, Benjamin SG (1997) Performance of different soil model configurations in simulating ground surface temperature and surface fluxes. Mon Weather Rev 125:1870–1884

Soares PMM, Cardoso RM, Miranda PMA, de Medeiros J, Belo-Pereira M, Espirito-Santo F (2012) WRF high resolution dynamical downscaling of ERA-Interim for Portugal. Clim Dyn 39:2497–2522

Solman SA, Sanchez E, Samuelsson P, da Rocha RP, Li L, Marengo J, Pessacg NL, Remedio ARC, Chou SC, Berbery H, Le Treut H, de Castro M, Jacob D (2013) Evaluation of an ensemble of regional climate model simulations over South America driven by the ERA-Interim reanalysis: model performance and uncertainties. Clim Dyn 41:1139–1157

Tack J, Barkley A, Nalley LL (2015) Effect of warming temperatures on US wheat yields. Proc Natl Acad Sci 112:6931–6936

Tahir ISA, Mustafa HM, Saad ASI, Elbashier EME, Elhashimi AMA, Abdeldaim MGA, Hassan MK, Gorafi YSA, Meheesi S, Idris AAM, Ibrahim HA, Eltayeb SM, Hamza FEA, Abdalla OS, Hamada AA, Abuelgassim AMA (2018) Grain Yield and Stability of Elite Stem and Leaf Rusts Resistant Bread Wheat Genotypes Under the Hot Environments of Sudan: A Proposal for the Release of Three Bread Wheat Varieties. National Variety Release Committee Meeting, 2 April 2018, Khartoum, Sudan.

Tahir ISA, Elahmedi AB, Ibrahim AS, Abdalla OS (2000) Genetic improvement in grain yield and associated changes in traits of bread wheat cultivars in the Sudan. In: The Eleventh Regional Wheat Workshop for Eastern, Central and Southern Africa. Addis Ababa, Ethiopia. CIMMYT. pp 60–66

Tahir ISA, Mustafa HM, Idris AAM, Elhashimi AMA, Hassan MK, Fadul EM, Kurmut AMA, Eltayeb SM, Meheesi S, Hassan AO, Abdalla OS, Assefa S (2020a) Enhancing wheat production and food security in Sudan through scaling up improved technologies using innovation platforms, Int J Agric Sustain 18:376–388

Tahir ISA, Elbashier EME, Ibrahim MAS, Saad ASI, Abdalla OS (2020b) Genetic gain in wheat grain yield and nitrogen use efficiency at different nitrogen levels in an irrigated hot environment. International Journal of Agronomy 2020: 9024671

Tao WK, Simpson J, McCumber M (1989) An ice–water saturation adjustment. Mon Weather Rev 117:231–235

Tariku TB, Gan TY (2018) Sensitivity of the weather research and forecasting model to parameterization schemes for regional climate of Nile River Basin. Clim Dyn 50:4231–4247

Taylor KE (2001) Summarizing multiple aspects of model performance in a single diagram. J Geophys Res Atmos 106:7183–7192

Tewari M, Chen F, Wang W, Dudhia J, LeMone MA, Mitchell K, Ek M, Gayno G, Wegiel J, Cuenca RH (2004) Implementation and verification of the unified NOAH land surface model in the WRF model. In 20th Conference on Weather Analysis and Forecasting/16th Conference on Numerical Weather Prediction, Seattle, WA, U.S.A., 12–16 January 2004.

Tiedtke M (1989) A comprehensive mass flux scheme for cumulus parameterization in large-scale models. Mon Weather Rev 117:1779–1800

Van der Linden P, Mitchell JFB (2009) ENSEMBLES, Climate Change and its Impacts: summary of research and results from the ENSEMBLES project. Met Office Hadley Centre, Exeter, UK, 160p

Wang XL, Feng Y (2013) RHtestsV4 User Manual. Climate Research Division, Atmospheric Science and Technology Directorate, Science and Technology Branch, Environment Canada. 28p

Wilby R.L, Wigley TML (1997) Downscaling general circulation model output: a review of methods and limitations. Prog Phys Geogr 21: 530–548

Xu CY, Zhang Q, El Hag El Tahir M, Zhang Z (2010) Statistical properties of the temperature, relative humidity, and net solar radiation in the Blue Nile-eastern Sudan region. Theor Appl Climatol 101:397–409

You L, Rosegrant MW, Wood S, Sun D (2009) Impact of growing season temperature on wheat productivity in China. Agric For Meteorol 149:1009–1014

Yuan X, Wood EF, Luo L, Pan M (2011) A first look at Climate Forecast System version 2 (CFSv2) for hydrological seasonal prediction. Geophys Res Lett 38: L13402

Zhang C, Wang Y, Hamilton K (2011) Improved representation of boundary layer clouds over the southeast Pacific in ARW-WRF using a modified Tiedtke cumulus parameterization scheme. Mon Weather Rev 139:3489–3513

Zhang N, Zhao C, Quiring SM, Li J (2017) Winter wheat yield prediction using normalized difference vegetative index and agro-climatic parameters in Oklahoma. Agron J 109:2700–2713

Zittis G, Hadjinicolaou P (2017) The effect of radiation parameterization schemes on surface temperature in regional climate simulations over the MENA-CORDEX domain. Int J Climatol 37:3847–3862

Zittis G, Hadjinicolaou P, Lelieveld J (2014) Comparison of WRF model physics parameterizations over the MENA-CORDEX domain. Am J Clim Chang 3:490–511

List of Publication

1. Title : Relationship of irrigated wheat yield with temperature in hot environments of Sudan

Authorship: Musa, A. I. I., Tsubo, M., Ali-Babiker, I. A., Iizumi, T., Kurosaki, Y., Ibaraki,Y., El-Hag, F. M. A., Tahir, I. S. A. and Tsujimoto, H.

Full Name of Scientific Journal with Volume, Number and Pages: Theoretical and Applied Climatology, Volume 145, Issue 3-4, Pages: 1113 – 1125 (DOI:10.1007/s00704-021-03690-1)

Published date : June, 2021

(Chapter 2)

2. Title: Evaluation of WRF Cumulus Parameterization Schemes for the Hot Climate of Sudan Emphasizing Crop Growing Seasons

Authorship: Musa, A. I. I., Tsubo, M., Ma, S., Kurosaki, Y., Ibaraki, Y. and Ali-Babiker, I. A.

Full Name of Scientific Journal with Volume, Number and Pages:

Atmosphere 2022, 13 (4), 572 (DOI:10.3390/atmos13040572)

Published date : April, 2022

(Chapter 3)